A major purpose of the Technical Information Center is to provide the broadest dissemination possible of information contained in DOE's Research and Development Reports to business, industry, the academic community, and federal, state and local governments.

Although a small portion of this report is not reproducible, it is being made available to expedite the availability of information on the research discussed herein.

LA-UR-84-3541

Los Alamos National Laboratory is operated by the University of California for the United States Department of Energy under contract W-7405-ENG-36

LA-UR--84-3541

DE85 008631

TITLE: SOLAR POND RESEARCH AT THE LOS ALAMOS NATIONAL LABORATORY

AUTHOR(S): G. F. Jones, K. A. Meyer, and J. C. Hedstrom
Los Alamos National Laboratory

D. P. Grimmer
New Mexico Solar Energy Institute
Las Cruces, New Mexico 88003

OK
DT

MASTER

SUBMITTED TO Jet Propulsion Laboratory
R. L. French
4800 Oak Grove Drive
Pasadena, California 91109

DISCLAIMER

Los Alamos Los Alamos National Laboratory
Los Alamos, New Mexico 87545

FORM NO. 836 R4
ST. NO. 2629 5/81

CONTENTS

ABSTRACT 1

I. PROGRAM DESCRIPTION 2

II. THE THEORY OF SOLAR PONDS 2
A. Interfacial Boundary Layer Model 2
B. Flux Ratio at a Boundary 4
C. Stability Issues 7
D. Models for Interface Motion and Pond Performance 9
E. Heat Extraction 11
F. Heat Loss to Ground 11

III. HYPOTHESIS AND DESCRIPTION OF THE DYNAMIC PERFORMANCE MODEL 12

IV. DESCRIPTION OF EXPERIMENTS 15
A. Pond-Simulation Tank Experiments 15
B. Flow Visualization Experiments 17
C. Full-Sized Experimental Salt-Gradient Solar Pond 18

V. RESULTS AND DISCUSSION 22
A. Flow Visualization - Laboratory Tank 22
B. Dynamic Performance Code Validation 22
C. Solar Pond Results 28

VI. CONCLUSIONS AND RECOMMENDATIONS FOR FUTURE RESEARCH 46

VII. DISPOSITION OF EXPERIMENTAL EQUIPMENT 47

ACKNOWLEDGMENTS 47

NOMENCLATURE 48

REFERENCES 49

SOLAR POND RESEARCH AT THE LOS ALAMOS NATIONAL LABORATORY

by

G. F. Jones, K. A. Meyer, and J. C. Hedstrom
Los Alamos National Laboratory
Los Alamos, New Mexico 87545

and

D. P. Grimmer
New Mexico Solar Energy Institute
Las Cruces, New Mexico 88003

ABSTRACT

A description of solar pond research at Los Alamos National Laboratory is presented. The main issues in the theory of solar ponds are discussed. Among these are the interfacial-boundary-layer model, models for interface motion and pond performance, heat extraction, and ground heat loss. The core of the research effort at Los Alamos was the development of a one-dimensional computer program to accurately predict dynamic performance of a solar pond. The computer model and the experiments that were designed and performed to validate it are described. The experiments include two laboratory tanks wherein temperature, salinity, and flow visualization data were obtained and a 232 m^2 outdoor solar pond. Results from preliminary validation show good agreement between the pond's predicted dynamic behavior and that which actually occurred in the experiments. More validation using data from full-sized solar ponds is needed. A new correlation for the ratio of interfacial salt-flux to heat-flux is proposed,

$$\frac{\rho c_p \beta F_s}{\alpha F_h} = 0.1455\, F_h^{-0.13},$$

which agrees well with our data. Recommendations for future research are given.

I. PROGRAM DESCRIPTION

The objective of the solar pond research program at Los Alamos was to obtain a thorough understanding of pond fluid dynamics. To this end, a coordinated experimental, analytical, and numerical program was planned. At the heart of the program was the development of a one-dimensional computer model capable of accurately predicting time-dependent solar pond temperatures, salinities, and interface motion.

When the program began, a major unsolved problem in salt-gradient solar ponds was the lack of a basic understanding of the mechanisms by which the various layer boundaries move and how to control them. To obtain a better understanding of layer motion, a series of flow-visualization experiments was conceived and performed. Two laboratory experiments and a full-scale outdoor solar pond were designed and built to provide quantitative data by which we could validate the model and enhance our understanding of pond dynamic behavior.

II. THE THEORY OF SOLAR PONDS

A. Interfacial Boundary Layer Model

The effectiveness of a solar pond is determined to a large extent by the thickness of the layers. The upper convecting zone (UCZ) absorbs solar radiation (Refs. 1, 2, and 3) but contributes no resistance to heat loss from the warm lower convective zone (LCZ); it is, therefore, desirable to minimize its thickness. The diffusive core (gradient zone) provides the pond's insulation, and reductions in its thickness below an optimal value will result in increased heat-loss rates. The thickness of the LCZ determines the amount of energy storage in the pond.

It is generally recognized that the boundaries separating the mixed (convective) zones and the diffusive core are not stationary, but move in response to forces acting on them. For reasons that are explained below, when there is an imbalance between the effects of convective stirring in the mixed zones and the diffusive flux of salt and heat through the core, the mixed zones can encroach upon the core, reducing its thickness and decreasing pond performance. The motions described here occur even though the diffusive core itself is hydrodynamically stable.

The physical process that governs interfacial motion in the region of the boundary between the LCZ and core in solar ponds is double-diffusive convection. This process also occurs at the interface separating the UCZ and the core, but may not be the major process in action. There, in addition to the effects of double-

diffusive convection, we encounter wind-induced convection and turbulence and effects caused by diurnal heating and cooling resulting in entrainment of the UCZ into the diffusive core.

Double-diffusive convection may occur in any fluid with the following characteristics: the fluid is composed of at least two species with different molecular diffusivities; and the species make opposing contributions to density. Here, the ratio of the thermal diffusivity to salt diffusivity is about 80. A good overview of ongoing research in the area of double-diffusive convection is presented by Huppert and Turner (Ref. 4).

The oceanographic community has done extensive work in the area of double-diffusive convection in thermohaline systems. Instead of the three-zone system of interest to solar pond researchers, the system studied by oceanographers consists of two convective zones separated by an interface across which exist step changes in salinity and temperature. The interface varies in thickness from a few millimeters to about five centimeters (Refs. 5 and 6). Thicker interfaces exhibit a nonconvecting core (in which molecular diffusion dominates) separated from convecting zones by regions of intermittent turbulent fluctuations. We regard these fluctuating regions as interface-boundary layers. Researchers have obtained empirical relations for fluxes of salt and heat through the interface as a function of the salinity and temperature steps across the interface.

A simple mechanistic model of the interfacial boundary layers of interest to oceanographers in which salt and heat transport are driven by thermally induced convection has been proposed independently by Lindberg and Haberstroh (Ref. 7) and Linden and Skirtcliffe (Ref. 8). The model assumes the simultaneous growth of a thermal boundary layer and a salinity boundary layer from a sharp interface (separating the intermittently turbulent LCZ and the diffusive core) into the LCZ. The steps of the model are depicted in Fig. 1. As time increases from zero, the thermal-boundary layer outdistances the salinity-boundary layer because the molecular diffusivity for heat is greater then that for salt. The growth of the boundary layers into the LCZ at time Δt is shown in Fig. 1. The density distribution within most of the thermal layer is unstable, and at some thickness Δx occurring at time t^*, the layer will break down and release a buoyant element. Subsequent turbulent mixing caused by this phenomenon restores local uniformity to the LCZ and the process of boundary-layer growth and breakdown continues in a periodic manner. The released element, which is called a plume or "thermal" (Ref. 9), is cooler and less salty than the bulk of the LCZ and gives rise to the

turbulent mixing within the LCZ. During the boundary-layer growth part of the process, as the boundary layers thicken, mass and energy conservation require that salt and heat pass into the diffusive core where they are transported upwards by diffusion. If we assume complete mixing of both boundary layers into the LCZ at the time of layer breakdown (Ref. 10), the ratio of the increase in potential energy of the system (caused by an increase in the elevation of salt mass) to the thermal energy transported through the interface may be estimated. This leads to a unique ratio of salt flux to heat flux (flux ratio). Oceanographic-model predictions of this ratio are in relatively good agreement with laboratory-measured values. The flux ratio is very important for two reasons: it plays a major role in predicting pond layer migration; it is also the correlating parameter used in the dynamic performance model described in th's report.

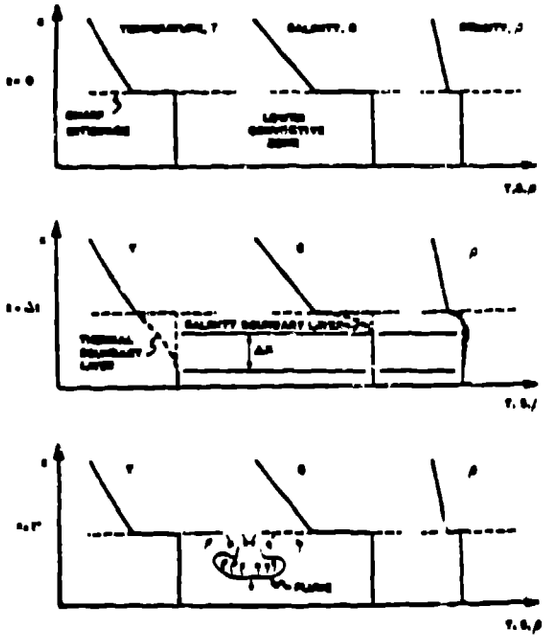

Fig. 1. Boundary layer model of double-diffusive convection of salt and heat.

B. Flux Ratio at a Boundary

Paramount among the assumptions made in the study of the oceanographic interface is that of quasi-equilibrium; at any instant in time, the properties of convection are the same that would be observed in steady state with the same values

of the flow parameters present at that time. Salt and heat storage effects in the interface regions and the core are thus neglected.

Turner (Ref. 11) has shown, through the use of dimensional arguments, that the flux ratio depends only on a quantity defined as the density-stability ratio, R_ρ, where

$$R_\rho = \frac{\beta \Delta S}{\alpha \Delta T} ,$$

where ΔS and ΔT are the step changes in salinity and temperature, respectively across the boundary. In particular, for $R_\rho \lesssim 2$, experimental evidence shows that the flux ratio decreases sharply with increasing R_ρ and for $R_\rho \gtrsim 2$, the ratio is a constant equal to

$$\frac{\rho C_p \beta F_s}{\alpha F_h} = \left(\frac{\kappa_s}{\kappa_t}\right)^{1/2} , \qquad (1)$$

where, for thermohaline systems, the right side is about 0.11. Piecewise-linear curve fits to data that support the existence of two distinct R_ρ regimes for the oceanographic boundary are presented in Fig. 2 (Ref. 11).

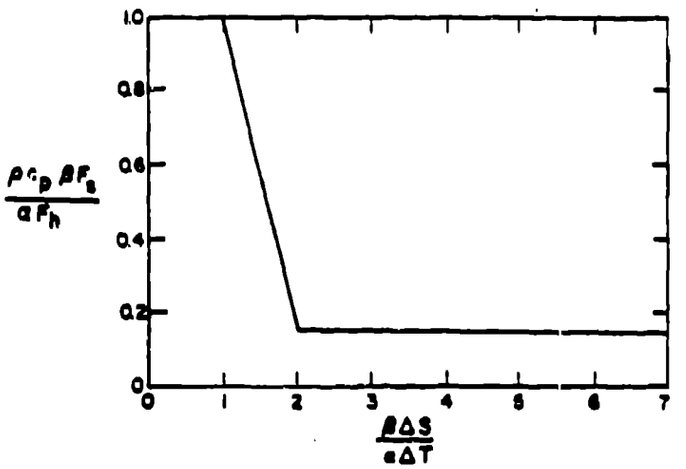

Fig. 2. Flux ratio vs R_ρ piecewise-linear fits from experimental data.

The regime for $R_\rho \lesssim 2$ is characterized by entrainment across the interface caused by wave motion and increased transport area. For the region $R_\rho \gtrsim 2$, double diffusive convection predominates. Interfaces in this regime are called diffusive interfaces. Typically, the interfaces in solar ponds are diffusive interfaces.

Equation (1) is also obtained by Turner (Ref. 12) and Linden and Shirtcliffe (Ref. 8), both of whom assumed the condition of marginal stability ($R_\rho = 1$) at the location where the step change in salinity and temperature occur. Experimental data of Marmarino and Caldwell (Ref. 6) and Crapper (Ref. 5) confirm the flux ratio expressed by Eq. (1) for high heat flux (greater than what would be encountered in solar ponds) but indicate an increased ratio for lower heat fluxes that is not predicted from Eq. (1). Newell and Von Driska (Ref. 13) and Newell (Ref. 14) have obtained the same result for the range of heat flux typical to solar ponds.

Mancini, et al. (Ref. 15) and Lindberg and Haberstroh (Ref. 7) both obtained the relationship

$$\frac{\rho C_p \beta F_s}{\alpha F_h} = \left(\frac{\beta \Delta S}{\alpha \Delta T}\right)_{\text{interface}} \left(\frac{\kappa_s}{\kappa_t}\right)^{1/2} , \qquad (2)$$

which for the case of marginal stability at the interface reduces to the result of Eq. (1). Equation (2) indicates an increase in the flux ratio as the density-stability ratio at the interface increases. We note that in most of our experiments, a well-defined interface was visible, presumably caused by a change in the index of refraction. This evidence suggests an overstable interface ($R_\rho > 1$) and from Eq. (2), flux ratios are greater than 0.11.

As discussed by Meyer (Ref. 16), because the heat flux in a solar pond is determined to a large extent by the large thermal resistance of the thick diffusive core, the small thermal resistances across the interfacial boundary layers are not important. Measurement of heat flux through oceanographic interfaces was performed by Marmarino and Caldwell, Linden and Shirtcliff, and Turner (Ref. 11). One result is notable, however. The usual representation of heat flux across an interface is the ratio of the actual heat flux to that which would occur across a thin, impermeable plane placed at the same location as the interface while maintaining the same temperature difference across it. Turner's results indicated that for $R_\rho \gtrsim 2$, the interfacial heat flux is smaller than its solid-plane value. He concludes that for this regime when the stabilizing salinity gradient impedes the flow of heat, a constant fraction of the potential energy released by the interfacial heat transport is used to transport salt upwards through the interface. This result supports the mechanistic boundary layer model of Lindberg and Haberstroh, and Linden and Shirtcliffe.

C. Stability Issues

The issue of stability in thermohaline columns was considered for the case of initial linear gradients in salt and temperature by Weinberger (Ref. 17), Veronis (Refs. 18 and 19) and Baines and Gill (Ref. 20) Stability within the core requires that not only the condition of static stability,

$$\frac{d\rho}{dx} < 0 \tag{3}$$

be satisfied, but the more stringent requirement of dynamic stability,

$$\left(\nu + \kappa_t\right) \alpha \frac{\partial T}{\partial x} + \left(\nu + \kappa_s\right) \beta \frac{\partial \rho_s}{\partial x} \geq 0 \quad , \tag{4}$$

must also be satisfied there.

Instabilities in the core caused by infinitesimal disturbances occur first as overstable oscillatory motions (wind-induced wave motion in UCZ and thermal expansion effects are two examples of perturbations that cause infinitesimal disturbances). In a system where the temperature and salinity are increasing downward, if a fluid particle is displaced an infinitesimal distance upward to a cooler, less-saline region, it will lose heat and salt by diffusion. Because of the large difference in diffusivities, it will cool rapidly, become more dense and be driven downward by its body force. Should viscosity effects be insufficient to dissipate the kinetic energy of this motion, the particle overshoots its equilibrium position and is directed back upward. This action can develop into a growing oscillation that leads to convection.

Stability of the core in the region of inclined side-wall boundaries has received little attention in the past. In the thermohaline case, a salt gradient must be zero at the impermeable side wall. Lateral density gradients within the core are formed near the walls that tend to drive the otherwise stable core fluid up at the walls (Ref. 21) and outward toward the center of the core. A system of interleaving convecting and nonconvecting layers is formed (Ref. 22). Disturbances from this motion could lead to the generation of local convective cells within the diffusive core and, thus, reduce its insulating value by increasing the rate of salt and heat transport upward.

Oscillatory motions within the core have been reported by Almanza and Bryant (Ref. 23) who conjectured that the motions result from overstable oscillations predicted from double-diffusive convection theory. Internal wave motion in the mixed zones at the interfaces between the mixed zones and the diffusive core in small laboratory tanks was noted by Grimmer and Jones (Ref. 24). The origin of this motion appears to result from the intermittent release of plumes predicted by the mechanistic convective breakdown model described above. However, disturbances did not affect the main body of the diffusive core because no convection was detected in it.

As discussed by Newell (Ref. 14), solar ponds operate at rather large values of R_ρ (>7), where R_ρ is the same as defined for thin interfaces. R_ρ defined in this manner may not be significant in solar ponds if nonlinear temperature or salinity gradients are present in the diffusive core because Eq. (4) shows that it is the local gradients (not those averaged over the core) that control stability and thus interface motion. Nonlinear salinity gradients in solar ponds and laboratory experiments are common and have been reported by Nielsen (Refs. 25 and 26) and Zangrando and Green (Ref. 27).

The existence of nonlinear gradients violates the quasi-equilibrium assumption made in the study of the oceanographic interface. In particular, a nonlinear salinity gradient indicates an imbalance between the rate of salt transport across the interfaces by double-diffusive convection and that transported through the core by molecular diffusion. In particular, if excess salt transport through the interface separating the LCZ and the diffusive core continues in time, the interface region becomes unstable and overturns. The overturning motion entrains some of the excess salt in the LCZ, restores stability to the interface, and results in encroachment of the LCZ upon the diffusive core. In this case, the interface is no longer in quasi-equilibrium, but is dynamic. The mechanistic arguments presented here are a first step in explaining the reduced flux ratios at increased heat fluxes as reported by Marmarino and Caldwell, Crapper (Ref. 5), Newell, and Newell and Von Driska. Thus, for a dynamic interface, the entrainment of excess salt stored above the boundary layers into the growing LCZ in combination with the near-constant rate of heat transport through the core causes a reduced ratio of the salt flux to heat flux. This effect should become more pronounced as the temperature gradient with its destabilizing effect is increased.

D. Models for Interface Motion and Pond Performances

Models for the dynamic motion of the interfaces in solar ponds have been proposed by Bergman et al. (Ref. 28) and by Meyer (Ref. 16). The former employs integral methods to solve for the temperature distribution and rates of mixed-layer growth but neglects the transport of salt across the interfaces and its effect on the reduced stability of the pond. The differences between predicted results and experimental data for salinity, temperature, and layer thicknesses were 20-30%.

Meyer (Ref. 16) presents a numerical model that uses empirical flux-ratios to predict time-dependent salinity and temperature, and interface motion. Preliminary attempts at validating the model showed good agreement between experimental and numerical results. Meyer included wind-driven turbulent entrainment in the UCZ based on the work of Crapper (Ref. 29) and Turner (Ref. 30). A study of the topic of wind-driven mixing in the UCZ in the absence of double diffusive convection at the core/UCZ boundary was presented by Atkinson and Harleman (Ref. 31). Their results indicated a possible reduction in annual average LCZ temperature of about 25% when wind-mixing effects occur.

A numerical model to predict the dynamic performance of the UCZ in solar ponds was presented by Cha, et al. (Ref. 32). Several analyses of solar pond thermal performance have been performed based on stationary interface boundaries -- notably by Kooi (Refs. 33 and 34), and by Hull (Ref. 35) for a pond whose bottom reflects diffusely. Among the numerical models developed under the assumption of stationary interface boundaries are those by Hull (Ref. 36), and Shah, et al. (Ref. 37); several solar pond design procedures are in this general category (Refs. 38 and 39). We note that results from models that consider only thermal behavior may be adequate for small time periods (say, a few days) over which little boundary-layer motion occurs but not for large time periods over which significant boundary-layer motion may exist.

The issue of interfacial stability in large-scale solar ponds was addressed by Newell and Boehm (Ref. 40). Based on limited experimental data they determined a criterion for stable interfaces as

$$\frac{\Delta S}{\Delta T} \geq 3.98 \times 10^{-3} \frac{wt\%}{^{\circ}C} \quad . \tag{5}$$

Equation (5) is expressed as the ratio of the salinity gradient to the temperature gradient based on linear profiles of both.

Nielsen (Refs. 41 and 42) presented the criterion,

$$\frac{G_T}{G_C^{1.6}} \leq 5 \times 10^{-3} \quad , \tag{5}$$

where G_T is the temperature gradient (°C/m) and G_C is the salinity gradient (kg/m^4). Equation (6) may be written in terms of the dimensionless flux ratio as

$$\frac{\rho c_p \beta F_s}{\alpha F_h} = 0.34 \times 10^{-3} \kappa_s \kappa_t^{-0.625} (\rho c_p)^{0.375} \beta\alpha^{-1} F_h^{-0.375} \quad , \tag{7a}$$

where F_h is the heat flux (W/cm^2). For 20% by weight NaCl at 60°C, Eq. (7a) becomes

$$\frac{\rho c_p \beta F_s}{\alpha F_h} = 0.0163 \, F_h^{-0.375} \quad . \tag{7b}$$

It is interesting to note that Nielsen's criterion requires a salinity gradient about an order of magnitude larger than that of Eq. (4).

Nielsen and Rabl (Ref. 3) performed a theoretical analysis to predict the threshold value of the daily heat absorbed in the LCZ necessary for LCZ growth. They also determined that the LCZ will shrink if the criterion

$$\alpha G_T < 0.22 \, \beta G_s \tag{8}$$

is satisfied. A comparison of the above stability criteria with the data from the Los Alamos solar pond will be presented in the section, Results and Discussion.

Research on gradient maintenance has been performed by Nielsen (Refs. 26, 42 and 44), and by Nielsen and Rabl (Ref. 43). They describe an injection procedure to modify the salinity gradient in the region of the interface to

maintain a thin UCZ while minimizing the rate of LCZ encroachment on the diffusive core. Annual rates of salt transport in their full-scale pond were measured at 10-20 kg/m^2-year.

E. Heat Extraction

Heat extraction from the LCZ and heat rejection to the UCZ in solar ponds has been studied by Jaluria (Ref. 45), and Jaluria and Cha (Ref. 46). Their analyses indicate that core entrainment into a forced flow in a mixed zone is characterized by the value of the overall Richardson number

$$Ri_0 = g \frac{\Delta\rho}{\rho_0} \frac{h_0}{U_m^2} \tag{9}$$

where $\Delta\rho$ is the density difference between the mixed zone and the incoming flow, h_0 is the mixed zone depth, and U_m the characteristic velocity in the mixed zone. For $Ri_0 > 0.85$ entrainment of the core into the forced flow is negligible.

The experimental results of Zangrando and Green (Ref. 27) for heat extraction in a large laboratory tank show LCZ interface erosion to be greatly increased at reduced values of R_ρ (defined at the interface) and for increased extraction velocities.

F. Heat Loss to Ground

The subject of ground conductivity and how it affects pond performance has received little attention. Heat and mass transfer through soils is a complicated process that includes the effects of molecular conduction, latent heat transport by pressure-driven vapor flow, and sensible heat transfer by the flowing liquid. Meyer and Hedstrom (Ref. 47) show conductivity to be very sensitive both to moisture (for moisture contents of 25% and less) and to soil composition (higher concentrations of sand vs. silt increase conductivity). Leboeuf and Johnson (Ref. 48) show significant effects of soil composition on the average annual LCZ temperature of a large pond. They indicate the need for more data on fundamental thermal-transport properties of soils before heat and mass transfer in soils can be adequately predicted. Fundamental studies of the physics of heat and mass transfer in soils has been done by deVries (Ref. 49) and Walker, et al. (Ref. 50).

III. HYPOTHESIS AND DESCRIPTION OF THE DYNAMIC PERFORMANCE MODEL

The primary thrust of the Los Alamos research effort in solar ponds is toward understanding the fluid dynamics and heat transfer within such ponds. To help accomplish this, a numerical model was developed to solve the one-dimensional, time-dependent diffusion equations for salt and heat transport in the pond.

For heat transport we have

$$\rho c_p \frac{\partial T}{\partial t} = \frac{\partial}{\partial x}\left[k_t \frac{\partial T}{\partial x}\right] + q(x,t) - L(x,t) \quad . \tag{10}$$

For salt transport, the governing equation is

$$\frac{\partial \rho_s}{\partial t} = \frac{\partial}{\partial x}\left\{\kappa_s \frac{\partial \rho_s}{\partial x} + \kappa_{st} \frac{\partial T}{\partial x}\right\} \quad . \tag{11}$$

The second term on the right side of Eq. (11) is the Soret term; it accounts for the transport of salt attributable to a temperature gradient. κ_{st} is the Soret diffusion coefficient. We use values of the Soret coefficient given by Rothmeyer (Ref. 51). In the diffusive core, the molecular diffusivity is used in Eqs. (10) and (11), whereas an eddy diffusivity is used if the region is convecting. The value of the eddy diffusivity chosen is large enough to ensure complete mixing. Salinity changes caused by evaporation and precipitation are not included in the model at present.

Our hypothesis is that boundary-layer behavior, such as that described in the theory section of the report, exists in ponds in the regions of the interfaces between the mixed zones and the diffusive core. We hypothesize that the boundary layers above and below a diffusive core are two halves of the thin interface layer that occurs at the temperature and salinity step of interest to oceanographers. Support for this conjecture comes from the observations of plumes descending from the LCZ boundary layer region in our laboratory-tank simulations of solar ponds (Ref. 52 and Fig. 5). Furthermore, we speculate that the flux relations obtained across the thin interface of the oceanographic studies also apply across a boundary layer separating the mixed zones and the core in solar ponds.

Consistent with the above hypothesis, static and dynamic stability criteria also apply. In our model, if Eq. (4) is not satisfied in a portion of the diffusive core, that portion is flagged as convecting and the appropriate eddy diffusivity is

used. If Eq. (3) is not satisfied across a boundary between a convecting region and the diffusive core, the convecting region encroaches on the core. The interface stability criterion, Eq. (3), is the same as that assumed by Turner (Ref. 12) in his analysis of a stable salinity gradient heated from below.

As discussed by Meyer (Ref. 16), because the major thermal resistance in the solar pond is that associated with the diffusive core, a correlation, such as that proposed by Marmarino and Caldwell for the interfacial heat flux driven by double-diffusive convection at the interfaces, is not needed. The heat flux is calculated from the mixed-zone temperatures and the core thickness.

The salt flux across an interface is related to the heat flux by an expression of the form,

$$\frac{\rho c_p \beta F_s}{\alpha F_h} = f(F_h) \quad , \tag{12}$$

where, in keeping with our hypothesis, the right side is the same empirical $f(F_h)$ relation that is obtained from flux measurements across a thin interface.

We believe that Eq. (12) applies across the solar pond boundary layers because in the quasi-equilibrium oceanographic studies, the flux ratio that is valid across the entire interface must be equally valid across each side of the interface and across the diffusive core separating each side. If this were not so, the quasi-equilibrium condition would be violated. We delay further validation of this hypothesis until the discussion of experimental and calculated results.

The numerical model includes a system of equations that accounts for wind-driven entrainment. Wind-driven entrainment acts in conjunction with double-diffusive convection at the boundary between the UCZ and the diffusive core.

We correlate entrainment of the diffusive core with the effect of wind shear by the relation,

$$\frac{U_e}{U^*} = C_1 Ri^{-n} \quad , \tag{13}$$

Where C_1 and n are empirical constants and U* is the frictional velocity that is directly proportional to wind speed. Ri is the local Richardson number and is defined by

$$Ri = \frac{gd^2}{\rho U^{*2}} \frac{\partial \rho}{\partial x} \quad , \tag{14}$$

Where $\partial\rho/\partial x$ is the density gradient in the diffusive core at the location where the core and UCZ meet.

We proceed to define salt and heat fluxes caused by entrainment from the following:

$$F_{te} = -U_e \rho c_p \Delta T \quad , \tag{15a}$$

$$F_{se} = -U_e \Delta \rho_s \quad . \tag{15b}$$

ΔT and $\Delta \rho_s$ are the changes in temperature and solute density across the boundary.

The fluxes from Eqs. (15) are superimposed on those calculated from the effect of double-diffusive convection alone. This assumption of separate, additive contributions from both the double-diffusive effect and the mechanical turbulence appears to be justified by our observations of the relatively rare mixing events in double-diffusive flows (Ref. 5) and similar observations by Turner (Ref. 30) for grid-generated turbulence.

The equations in the model are solved simultaneously by first writing them in their finite-difference forms and then solving the resulting system of linear algebraic equations by an implicit method. The mesh size used in the finite difference scheme was one centimeter.

A more detailed description of the model is given in Meyer (Ref. 16).

IV. DESCRIPTION OF EXPERIMENTS

To obtain a deeper understanding of the fluid motion in the region of the boundary layers and within the mixed zones of solar ponds, we designed, built, and instrumented two laboratory tanks and a full-sized outdoor pond. Data from these experiments were also used to initiate validation of the dynamic performance model.

A. Pond-Simulation Tank Experiments.

The first phase of our laboratory program involved the development of a pond-simulation tank to obtain quantitative data for code validation. It consisted of a glass dewar, 29-cm i.d. and 75-cm deep with a bottom heater and a thermoelectrically cooled heat exchanger on top to establish the desired temperature gradient. To simulate a one-dimensional section of a solar pond it is necessary to minimize radial heat loss. This was accomplished by using a series of guard heaters independently controlled (by differential thermocouples) that maintained the outside wall of the dewar at the same temperature as the fluid within. The outside surface of the guard heater assembly was insulated with a minimum of 10 cm-thick polystyrene insulation.

A rake supporting two 100-ohm platinum resistance thermometers (RTDs) and two platinum point-conductivity probes was used to measure temperature and salinity.* The RTDs were glass encapsulated and had an outside diameter of 0.8mm to provide near-pointwise temperature measurement. RTDs were chosen for this experiment because of their greater sensitivity and reliability compared with other thermometers. RTD resistances were measured using a 4-wire potentiometric circuit with a high-impedence digital voltmeter.

The point-conductivity probe used in the experiment described here was developed at Los Alamos because of the need for accurate, high spatial resolution, in situ salinity measurements over a broad salinity range (Refs. 53, 54 and 55). A schematic diagram of a point conductivity probe is shown in Fig. 3. Basically, the probe consists of a length of platinum wire 0.51 mm in diameter encased in a 2-mm-o.d. glass tube to expose only the tip of the platinum wire. This asssembly

---

* Initially, to determine if any radial or circumferential temperature gradients existed, we measured temperature using five RTDs equally spaced on a rake having two horizontal, mutually perpendicular legs extending radially to the inside wall of dewar. No significant temperature variations were found.

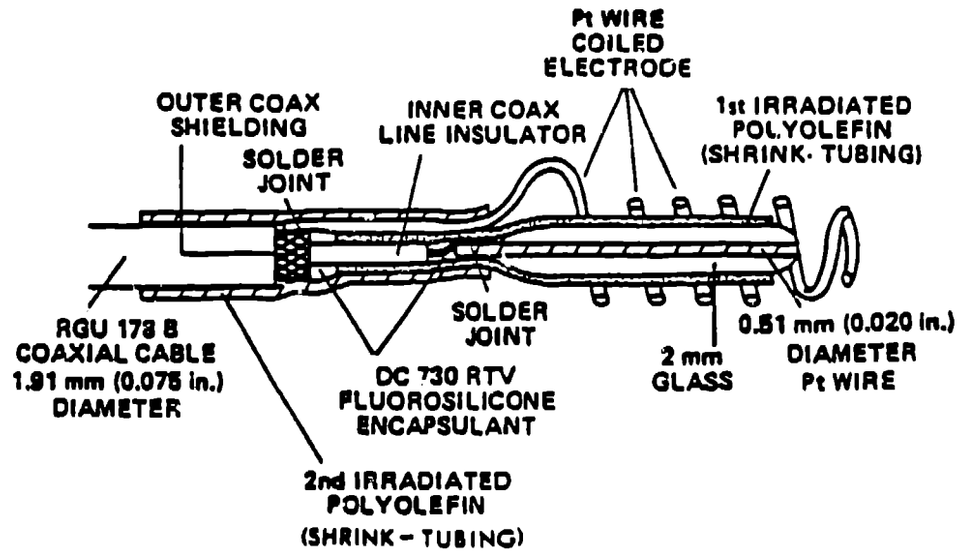

Fig. 3. Point-Conductivity probe schematic diagram.

is covered with an RTV fluorsilicone that is then sealed from salt water intrusion by a length of shrink tubing. A spiral-wound secondary electrode of large surface area surrounds the platinum tip. Point-conductivity measurements are obtained as a small electric current flows between the two electrodes. The current density at the probe tip is much greater than that at the secondary electrode because of the large difference in surface areas. The resulting electrical conductivity measurement is, thus, more heavily weighted in the region of the tip than elsewhere.

Before use, the platinum probe tip was first platinized using a Beckman model PK-1A platinizing kit.* The platinized coating reduces the rate of deterioration of the exposed probe tip and provides more stable and precise conductivity readings.

During each experiment, the probe was calibrated in situ by extracting a minimum of four samples from the tank. The samples were withdrawn using hypodermic needles or stainless steel capillary tubes at the same horizontal location as the probe tip and at the same time the conductivity was measured. The specific gravity of each sample was then measured (after it cooled to room temperature) by a Mohr-Westphal balance accurate to ±0.0001.

---

* Beckman Instruments Inc., Cedar Grove, New Jersey 07009.

The rake supporting the RTDs and point-conductivity probes was automatically driven through the tank at a prescribed time during the day at a rate of about 1 cm/min. One traverse per day was taken, but in situ calibration was performed only every three or four days to minimize disturbing the layer by extracting and reinjecting samples of fluid. On the days when calibration was performed, a salt balance was calculated for the LCZ and UCZ between that day and the day of the last calibration, and the average salt flux through the interfaces estimated for that period of time. The heat flux was determined from the local slope of the temperature profile. Data was automatically taken by a HP 9830 computer and data acquisition system and stored on magnetic tape for future reference.

B. Flow Visualization Experiments

The second phase of our laboratory experimental program consisted of flow-visualization experiments aimed at a detailed understanding of the flow patterns near the boundary layers. In addition, we also obtained quantitative temperature and salinity measurements to supplement those from the dewar experiments. This study was carried out in a bottom-heated plastic tank of approximate dimensions 30cm x 30cm x 75cm-deep (Ref. 52). The sides and bottom of the tank were insulated. Sections of the side insulation were removable to permit us to observe the flows and to photograph them.

After searching for an appropriate flow-visualization technique wherein we considered shadow graphs, dye markers (Ref. 56), and hydrogen bubbles, we decided on using thymol blue as a fluid particle tracer (Ref. 57). Thymol blue is a Ph indicator, and solutions containing small concentrations of it will change color locally by the creation of ions in the region of a charged electrode. A grid electrode (about 10-cm square), made up of fine tungsten wires, was suspended about 1cm below the LCZ interface for experiments performed in the LCZ and immediately above the UCZ for experiments performed in that zone.

To obtain local salinity and temperature data, a point-conductivity probe and a type-T thermocouple (suitably protected from salt water attack) were installed at the end of a long tube that was manually traversed through the tank. A series of movable extraction ports were installed in one of the tank walls to accomodate point probe calibration. During extraction, the probe tip and the extractor port were aligned by using a cathetometer.

C. Full-Sized Experimental Salt-Gradient Solar Pond

The primary purpose of our experimental pond is to provide a mechanism for full-scale validation, under controlled but realistic conditions, of our numerical model. A detailed description of the pond design and construction is given in Jones, et al. (Ref. 58) and Jones and Meyer (Ref. 59) and only a brief summary of it is given here.

A unique feature of the pond is its excavation not from sand or clay soil, as with other ponds, but from a lightweight porous rock known as "tuff"; such rock forms the the major fraction of the Los Alamos area surface geology. Tuff has a relatively small thermal conductivity, which implies that little, if any, insulation is necessary to reduce perimeter heat losses. In addition, because tuff is relatively strong, it was possible to build a pond with vertical side walls and minimize the problem of localized convection that could occur if the sidewalls sloped. Because of these features, the salt and heat transport in our pond was expected to be truly one dimensional.

The construction of the 232 m^2 by 3.5m-deep pond was begun in October 1981. After excavation, the pond walls were covered with an 8-cm thick layer of polyurethane insulation, mostly to smooth the rock surface and prevent a possible liner tear. A back-up liner of 0.5-mm-thick, rolled-on Hypalon (on the walls) and a 0.5-mm-thick sheet of PVC (on the bottom) was installed after 15 cm of smooth plaster sand was spread evenly on the rock floor. Another layer of sand covered the PVC, in which we embedded four electric resistance leak detectors. The main liner was 1.2-mm-thick fiber glass-reinforced Hypalon installed in three pieces and joined in the field. To accomodate settling, we delayed anchoring the edges of the main liner in the ground until the pond was filled. Six perimeter heat flux meters were installed in the tuff before beginning insulation work -- one in each wall and two in the pond floor.

Instrumentation at the pond consists of an underwater pyranometer (Eppley model 8-48) and traversing and fixed salinity- and temperature- measuring probes. The traversing device consists of a wheeled trolley driven vertically by a wire at a rate of 0.9 cm/min. through the pond; the trolley rides on a rectangular rail. Installed on the trolley are two platinum RTDs, an induction salinometer (Beckman CEL-RAS7 with a RIS5 indicator), and a platinum point-conductivity probe.

Typically, one traverse per day was run; each traverse provided temperature and salinity data at increments of 0.8 cm. The fixed probe consists of a rake supporting 28 type-T thermocouples and 28 sample-fluid withdrawal ports located every 10 cm. The ports permit in situ calibration of the point probe installed on the traversing trolley. The instrumentation rakes were stabilized by supports from a catwalk that extended over the pond from one of its banks. The material of construction was 316 stainless steel nearly throughout. No welding was done on metals to be submerged in the pond and bending of materials used for components that would be submerged was minimized to reduce the possibility of accelerated corrosion.

The initial gradient of 120 cm was established on August 4, 1982. The initial LCZ and UCZ thicknesses were 120 cm and 20 cm, respectively. The pond began warming rapidly with the LCZ initially at 25°C and 18.5% salinity. The rate of temperature increase in the LCZ was 1.2°C/day for the first month of operation, decreasing to 0.25°C/day for the second month.

At the end of the first week in September, we began to notice an abnormal drop in the surface level of the pond and suspected a leak. A graph of the salinity profiles over the period when the leak began is shown in Fig. 4.

In Fig. 4 we note the thickness of the core (gradient zone) is the same for August 31 and September 21, however its location is about 13 cm lower on the later day. We see further evidence from inspecting Fig. 5, where the depths of various isosalinity planes in the core are shown as a function of time. In Fig. 5 there is a negative slope to all curves after September 1. We concluded that the leak was in the LCZ. Subsequent calculations of salt inventories within the pond indicated a leak rate of about 1.8 m^3/day.

After cleanup of the excess salt on the bottom of the pond, removal of the catwalk and baseplate, and cooling the pond, two divers descended to inspect the liner in the LCZ region. They found a one-cm-long hole in the crease of the liner where the north wall and the floor meet. The tear was not in a seam. We presume that the tear was caused by excessive stress during settling of the pond bottom and we indicate below two independent effects that may have led to the high stress in the liner. First, the combination of hydrostatic pressure and high temperatures from large solar radiation intensities on the north wall caused the back-up and main Hypalon liners to stick together. The needed slippage of the main liner was thus prevented and large stresses at the bottom resulted. A similar stress tear had occurred on the west wall above the waterline sometime after the one in the LCZ and was repaired. Sticking was evident along that wall also. Second, because of

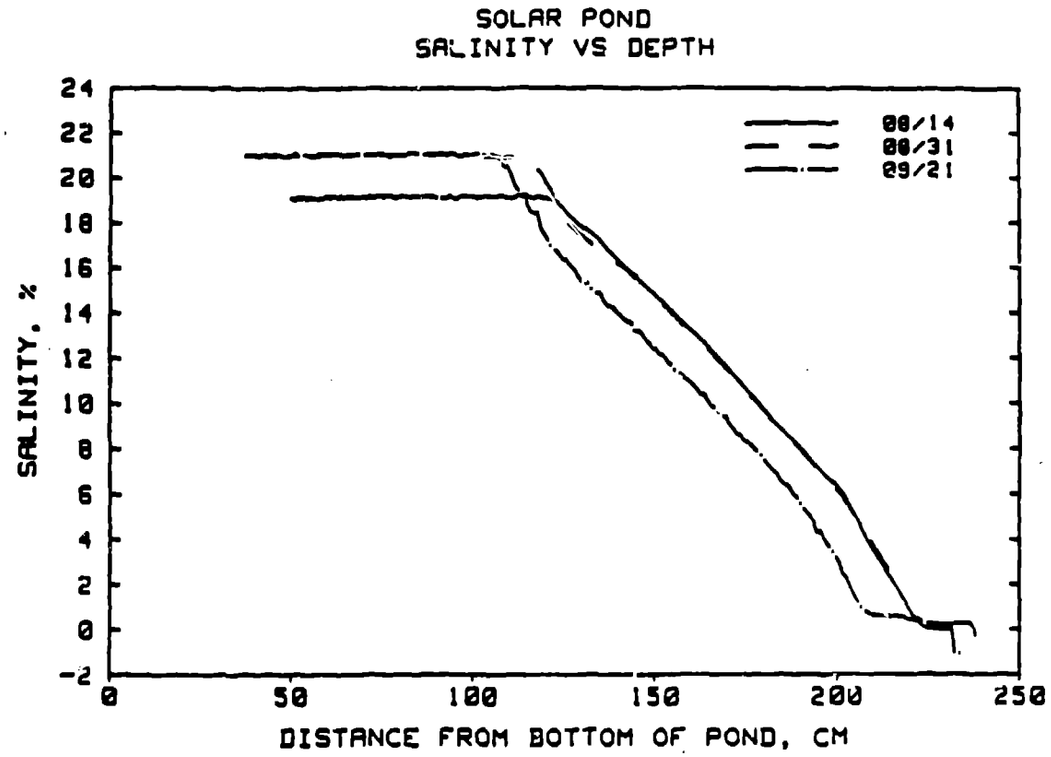

Fig. 4. Salinity profiles for solar pond.

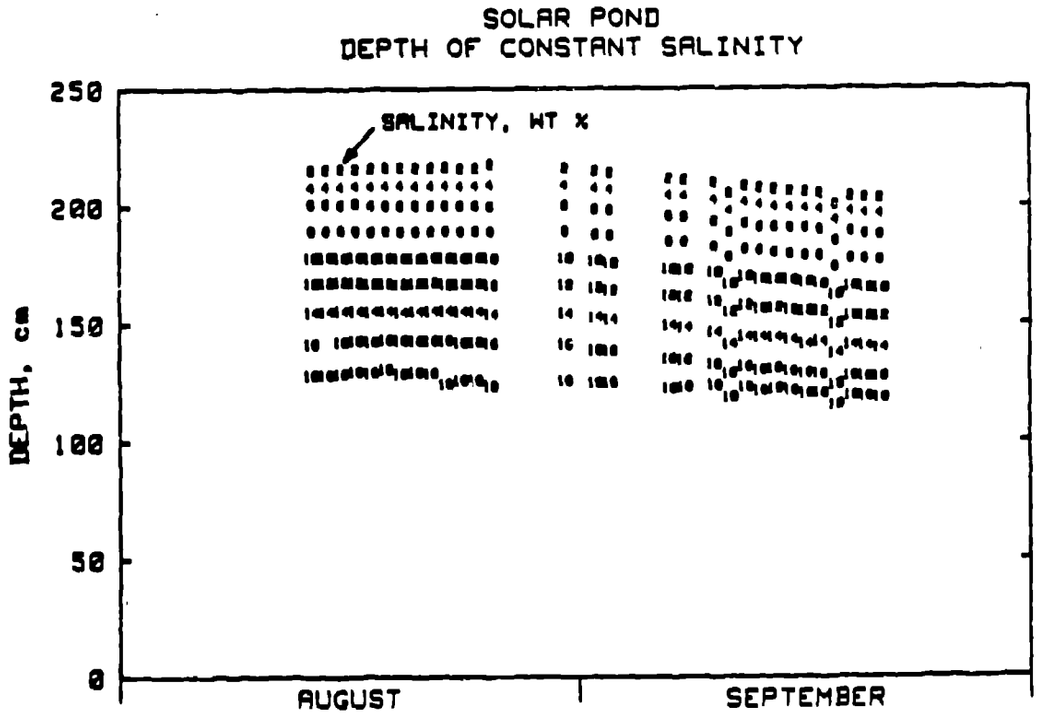

Fig. 5. Isosalinity-plane depth as a function of time.

the harsh environment into which the Hypalon liner was to be put, the supplier of the liner recommended fiberglass reinforcing for additional strength. Polyester is the standard reinforcement. Fiberglass, however, has very little ductility compared with polyester. We believe the lack of ductility in a region where it was needed contributed to the tear.

After two attempts, the divers repaired the leak by putting two hypalon patches on it and using a "5-minute" epoxy as a bonding agent. Sandbags were placed over the repaired area as added insurance. We arrived at the decision to use epoxy after evaluating the results of numerous underwater patching tests performed in the laboratory.

Another problem arose early in June 1983. For some reason, gas began to seep from the rock beneath the pond forcing the main liner upwards toward the surface. About a dozen gas bubbles under the liner were noted over a 3-week period. Their heights ranged from several cm above the floor to one that forced the liner through the surface of the pond. All of the large bubbles were removed by pushing down on them from above and pushing them toward a corner where a small incision in the liner had been made on the bank. The origin of the gas remains uncertain. A gas analysis showed it to be nitrogen-rich air possibly displaced from the porous tuff by unusually large mountain run-off earlier in the year or from the air displaced by the brine from the liner leak 6 months earlier. The appearance of the few smaller bubbles that were left in the liner has not changed since the end of June 1983.

One unfortunate result of the gas problem was another tear in the liner. It again occurred at the base of the north wall. Rather than cooling the pond, we attempted to patch the hole from above water. A double-sided, tar-like tape supplied to us by L. Wittenberg of the Mound Facility, Miamisburg, Ohio, was applied to the bottom of a stainless-steel plate. After cleaning the pond liner in the region of the tear with steel wool, we lowered the plate onto the area, tamped it into place, and placed sandbags on top of it. The water level of the pond stabilized after the patch was applied.

V. RESULTS AND DISCUSSION

A. Flow Visualization - Laboratory Tank

Figure 6 shows a photographic sequence of flow patterns immediately below the interface separating the LCZ and the diffusive core. Photographs were taken at 5 second intervals. Plumes of cool, less salty, dyed water are clearly visible as they descend from the interface. Patterns of this type were repeatedly observed for the cases where the effects of bottom heating did not disturb the interface. A structure such as that shown in Fig. 6 agrees very well with the break-down processes assumed in the mechanistic model.

At large rates of bottom heating, the convection generated at the heating plate directly influences the flow at the interface separating the LCZ and the core. The flow patterns immediately below this interface under the condition of large bottom heating are shown in Fig. 7(b). Fig. 7(a), which shows fluid motion below the interface with no bottom heating, is included for comparison. We note in Fig. 7(b) that the plume structure has been replaced by whisps of fluid being swept away by the convective stirring within the LCZ. We believe this influence may cause an increase in the rate of salt transport through the boundary and result in an increased flux ratio. The oceanographic model for the interface assumes that the convective motions in the neighborhood of the interface are caused solely by the effect of heat transport through the interface. Thus, interfacial salt and heat transport caused by convection arising from sources other than plume motion are neglected in the model.

Quantitative measurements with thymol blue have proved difficult. During observations made with heat fluxes in the range of 50 to 90 W/m^2, plume velocities ranged between 0.1 and 0.2 cm/s. The average plume velocity appeared to increase with heat flux; plume spacing ranged from 3 to 6 cm.

B. Dynamic Performance Code Validation

Our first attempt at validation was to use the numerical model to reproduce the experimental results obtained by Purdue University investigators (Ref. 60) in a bottom-heated, solar-pond simulation experiment. Details of the comparison are presented in Meyer (Ref. 16). Figures 8 and 9 compare our calculations with experimental data; agreement is good. Figure 8 indicates that the model reproduced the motion of the interfaces very well during the time the mixed zones were advancing into the diffusive core. In Fig. 9, good agreement is also shown between the calculated and experimental temperature histories in the mixed zones.

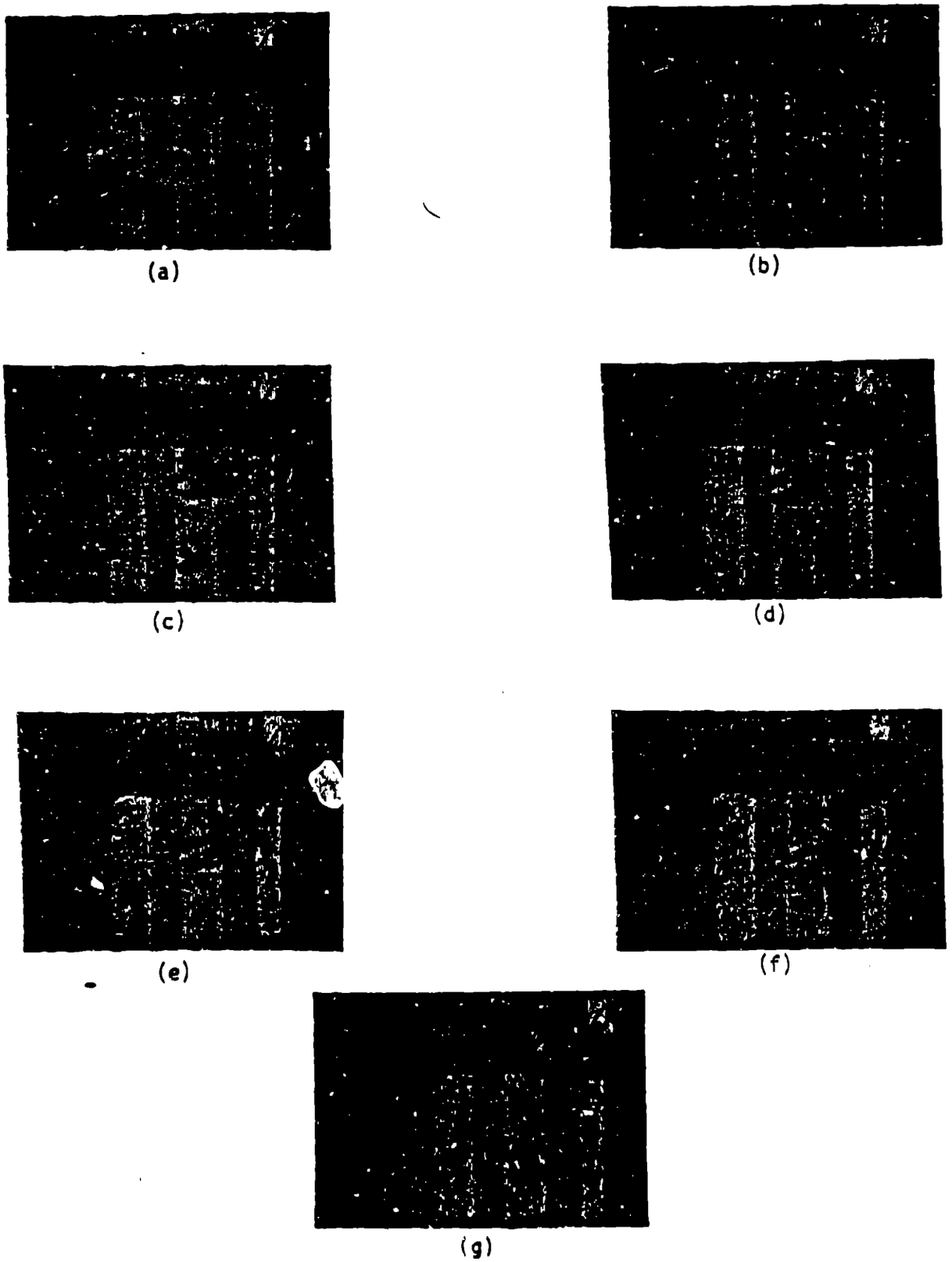

Fig. 6. Flow patterns just below interface separating the diffusive core and lower convective zone with small bottom heating. Sequence was photographed at 5-second intervals.

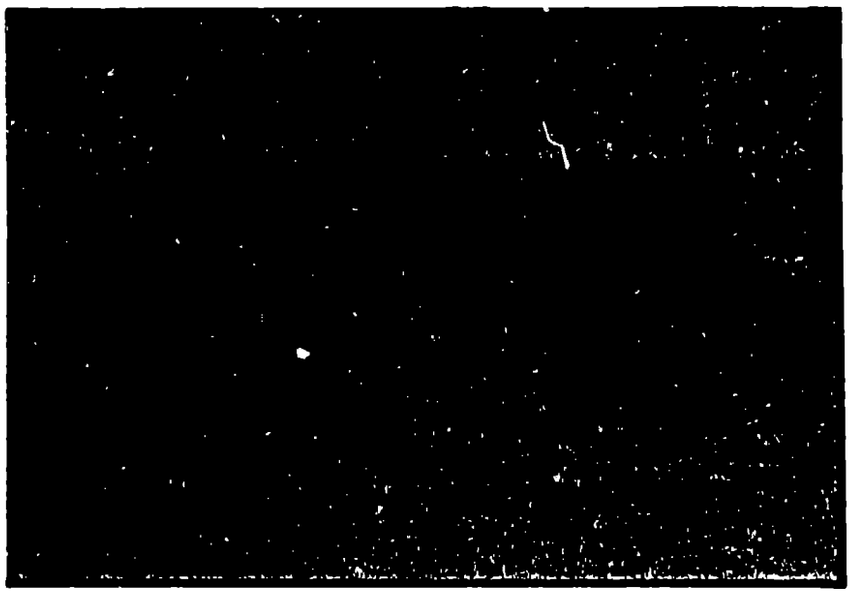

(a)

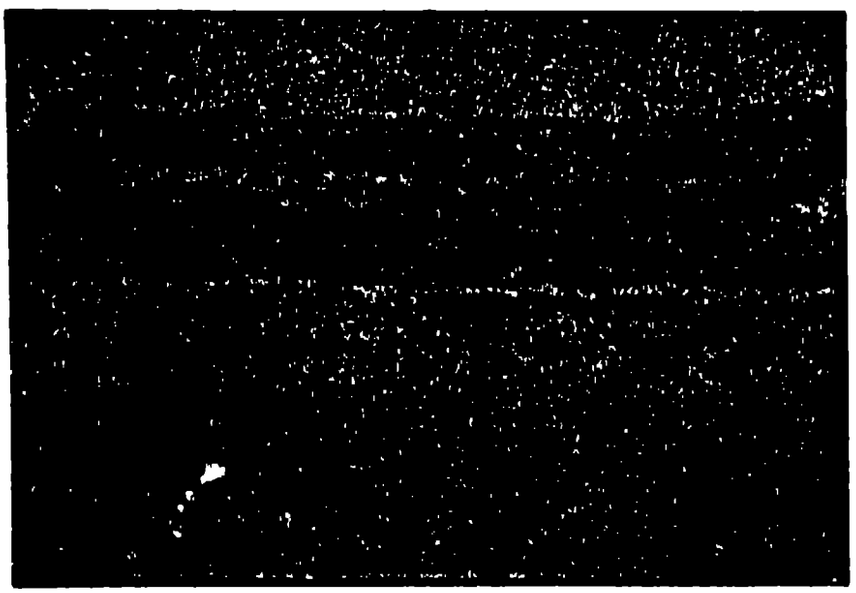

(b)

Fig. 7. Flow pattern just below interface separating the diffusive core and lower convective zone (a) with heater off and (b) with heater on.

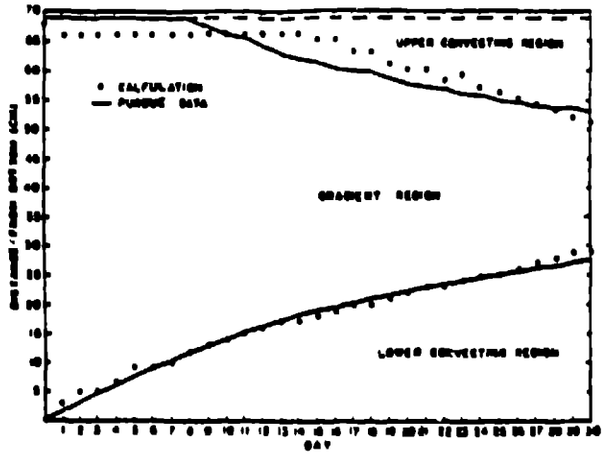

Fig. 8. Layer positions versus time.

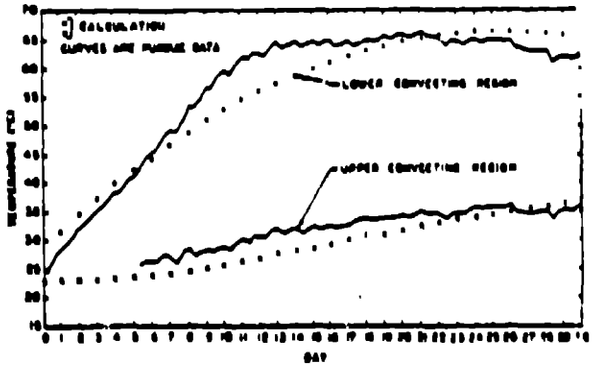

Fig. 9. Convecting zone temperature versus time.

To obtain a good match to the experiment above, it was necessary to modify Eq. (7b) to

$$\frac{\rho C_p g F_s}{\alpha F_h} = 0.1455\, F_h^{-0.13} \quad . \tag{16}$$

Equation (16) gives flux ratios larger than those from Eq. (7b) but remains within the range of Marmarino and Caldwell data and Los Alamos data yet to be presented.

We have used our wind-entrainment, double-diffusive model [Eqs. (13) through (15)] to calculate the performance of the Miamisburg, Ohio, solar pond over a 3-month period. Details of the comparison are described in Meyer et al. (Ref. 52).

There is some uncertainty regarding the appropriate values of C_1 and n in Eq. (13). We tried two sets of values in our calculations. The values of C_1 = 0.075 and n = 1 were obtained by Wu (Ref. 61) and the values C_1 = n = 3/2 were obtained by Kit, et al. (Ref. 62). Observed and calculated interface positions as a function of time are shown in Fig. 10. We note that the calculation with n = 1 gives good agreement with observations for the UCZ and LCZ; the use of n = 3/2 underestimates the growth of the UCZ.

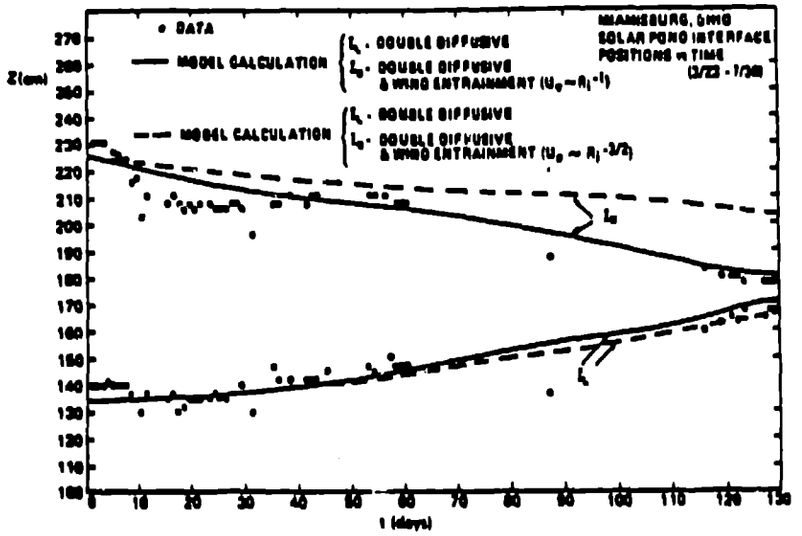

Fig. 10. Comparison of the measured and calculated interface positions for the Miamisburg solar pond.

The correlating parameter in the numerical model is the flux ratio. The object, when comparing the calculated results from the model with those from our experiments, is to calculate the flux ratio from experimental data and, by using this flux ratio in the code, attempt to match the performance observed in the experiment.

We obtain an expression for the time-averaged salt flux from

$$F = -U_1 \rho_s + \kappa_s \frac{\partial \rho_s}{\partial x} \quad , \tag{17}$$

where F is the net instantaneous salt flux (g/cm^2-s) and U_i is the instantaneous boundary velocity (cm/s).

Equation (17) may be integrated over time from t_1 to t_2 to obtain

$$\Delta M_s \equiv \int_{t_1}^{t_2} F\, dt = -\int_{t_1}^{t_2} U_i \rho_s\, dt + \int_{t_1}^{t_2} \kappa_s \frac{\partial \rho_s}{\partial x}\, dt \quad ,$$

or

$$\frac{\Delta M_s}{\Delta t} = \frac{-\bar{\rho}_s}{\Delta t} \int_{t_1}^{t_2} U_i\, dt + \overline{\kappa_s \frac{\partial \rho_s}{\partial x}} \quad . \tag{18}$$

In Eq. (18), the overbar indicates a time-averaged quantity and M_s is the mass of salt per unit of pond area.

With

$$U_i = \frac{dx}{dt} \quad , \qquad \frac{\Delta M_s}{\Delta t} = \frac{M_{st_1} - M_{st_2}}{\Delta t} \quad ,$$

Eq. (18) becomes

$$\overline{\kappa_s \frac{\partial \rho_s}{\partial x}} = \frac{M_{st_1} + \bar{\rho}_s \left(x_{t_2} - x_{t_1}\right) - M_{st_2}}{\Delta t} \quad . \tag{19}$$

The numerator in Eq. (19) is the difference in salt inventories (per unit area) in the mixed zones at times t_1 and t_2, respectively plus a contribution from the product of the time-averaged density at the interface and the distance over which the interface moves in time Δt.

We use Eq. (19) to calculate salt fluxes in our experiments. The salinity values in the mixed zone are obtained from the measured densities of the extracted samples. The values of the heat fluxes are obtained from the local temperature gradients in the region of the interface under consideration.

Our largest source of error was in determining the position of the interface. The salinity-profile data were scattered whereas the temperature profiles were smooth and rounded in the region of the interface. We defined the interface as the intersection of the straight-line extension of the temperature profile in the core and the constant temperature line of the mixed zone. An error range in the flux ratio arises from uncertainties in the location of the interface and the value of the temperature gradient. Property data is from Elwell, et al. (Ref. 63).

A comparison of the data from the tank experiments with calculations is presented in Figs. 11-18. Time-dependent LCZ salinity, temperature, interface location, and UCZ salinity, and interface location are shown. Notable results are summarized in Table I. The duration of the experiments ranged from 12 to 22 days, and heat fluxes ranged from 8.8 to 61.2 W/m^2. Included on each figure are the heat flux and the dimensionless flux ratio used in the model to produce the calculated results as shown. We note that in all cases, the heat flux and flux ratio used in the model fall within the error range of the tank data. We further note that good agreement between the calculated and experimental results is obtained by using these values.

The anomalous behavior of the LCZ temperature history in Fig. 16 occurred when, in error, we accidentally increased the rate of bottom heating slightly on the twelfth day of the experiment. The discontinuity in heating was included as input to the model for this case and from Fig. 16, we note that the model predicts the correct temperatures even after the sudden change of heating rate occurred.

From the results presented in Figs. 11-18, and the good agreement observed between calculated and predicted results, it appears that the model contains the features necessary to predict time-dependent salinity, temperature, and motion of the mixed layers.

C. SOLAR POND RESULTS

The 232-m^2 solar pond was operated in a run-down mode (no heat extraction or gradient maintenance) for the period from June 1 to August 18, 1983. The primary purpose of the experiment was to obtain flux-ratio data for a full-sized pond and compare them with those data obtained from the small-scale laboratory experiments. Because the experiment was not funded, model validation would be done only if sufficient time could be spared from other projects, or if personal time could be found.

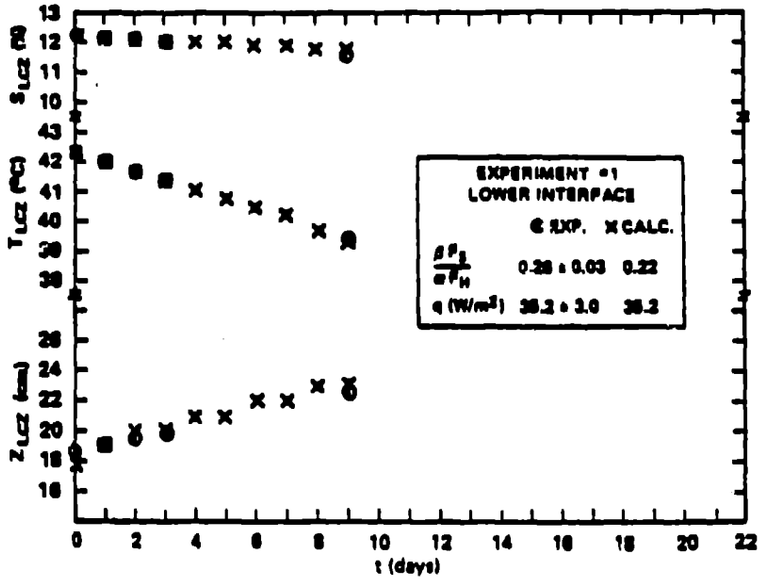

Fig. 11. Comparison of observed and calculated results for laboratory tank experiment number 1. Z = height of boundary layer above pond bottom. $F_H = F_h/\rho c_p$.

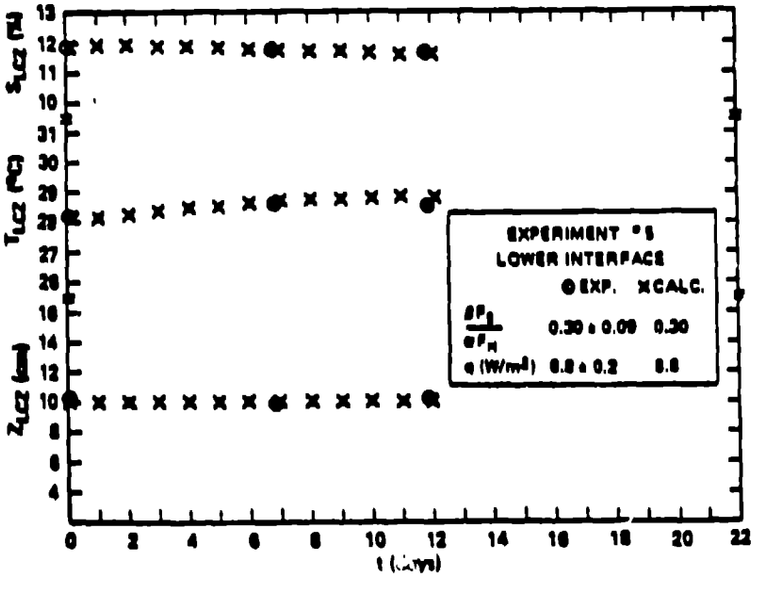

Fig. 12. Comparison of observed and calculated results for laboratory tank experiment number 5. Z = height of boundary layer above pond bottom. $F_H = F_h/\rho c_p$.

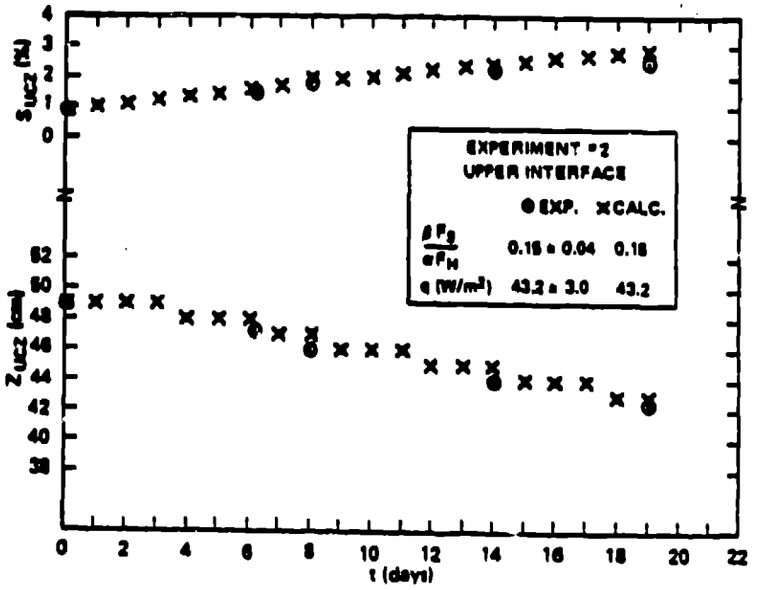

Fig. 13. Comparison of observed and calculated results for laboratory tank experiment number 2. Z = height of boundary layer above pond bottom. $F_H = F_h/\rho c_p$.

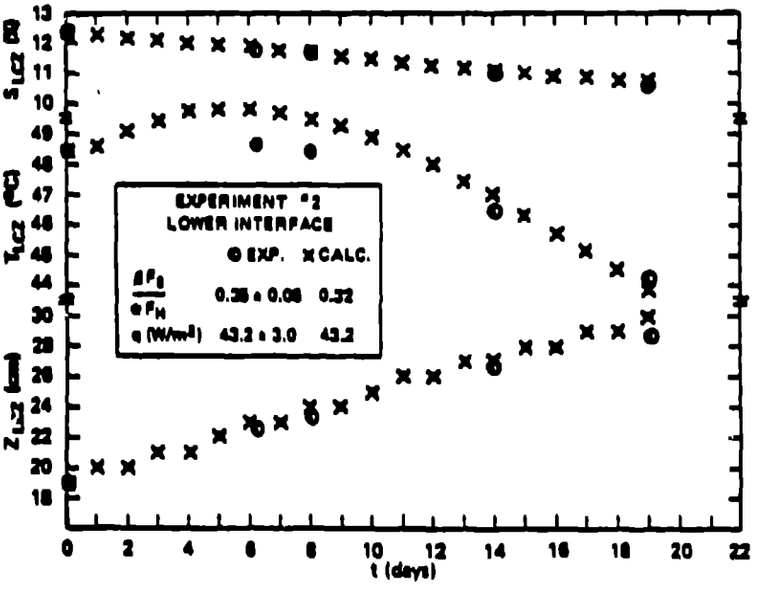

Fig. 14. Comparison of observed and calculated results for laboratory tank experiment number 2. Z = height of boundary layer above pond bottom. $F_H = F_h/\rho c_p$.

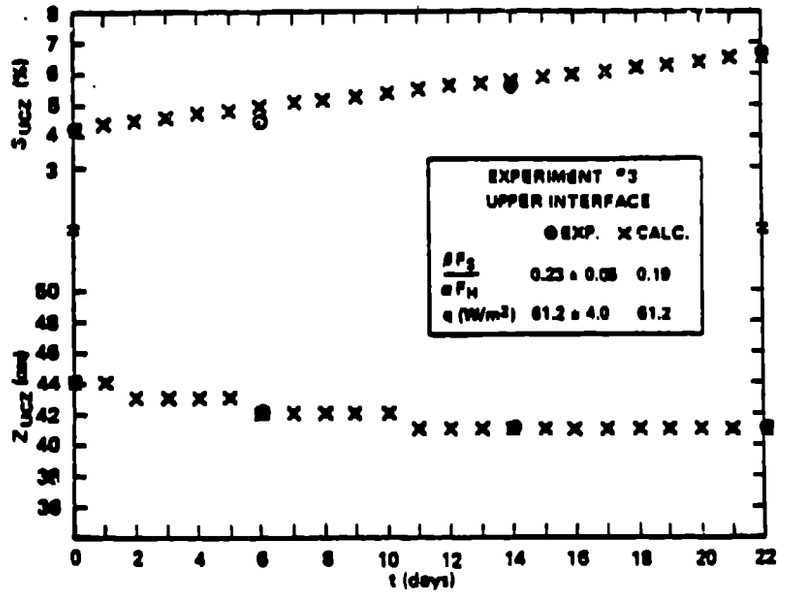

Fig. 15. Comparison of observed and calculated results for laboratory tank experiment number 3. Z = height of boundary layer above pond bottom. $F_H = F_h/\rho C_p$.

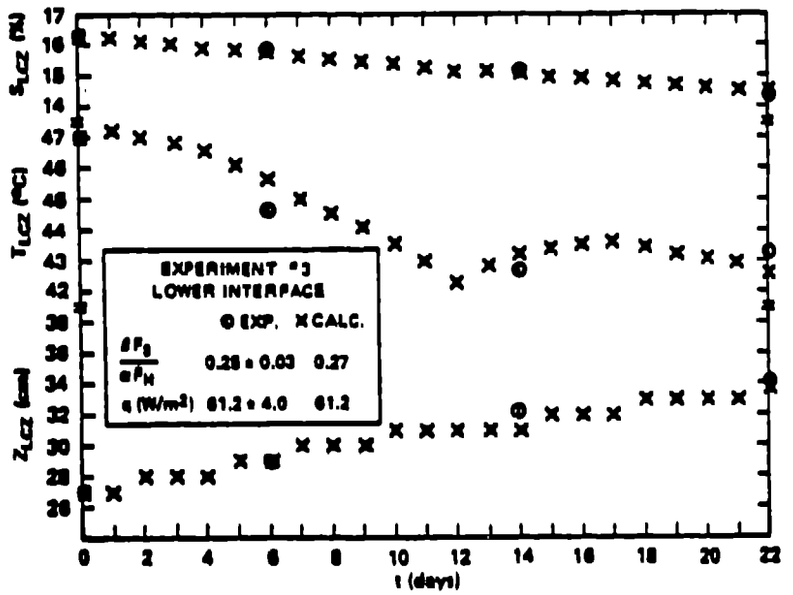

Fig. 16. Comparison of observed and calculated results for laboratory tank experiment number 3. Z = height of boundary layer above pond bottom. $F_H = F_h/\rho C_p$.

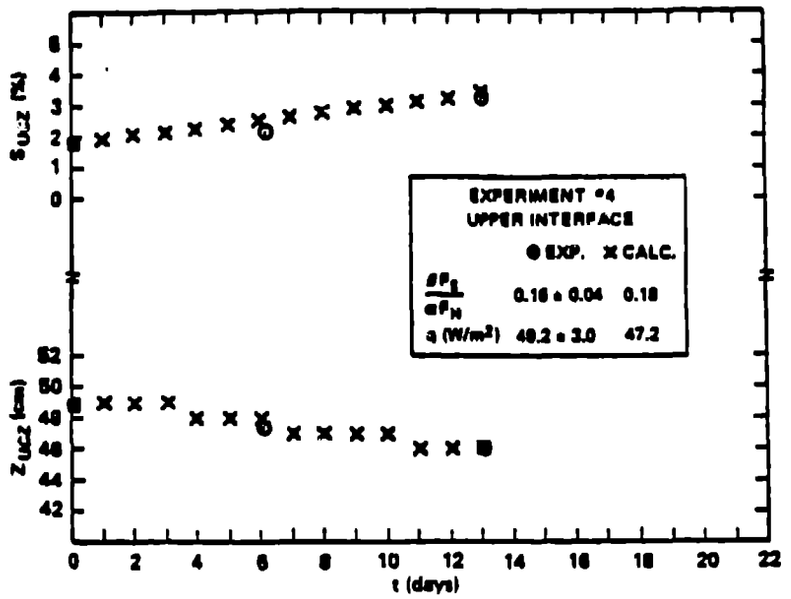

Fig. 17. Comparison of observed and calculated results for laboratory tank experiment number 4. Z = height of boundary layer above pond bottom. $F_H = F_h/\rho c_p$.

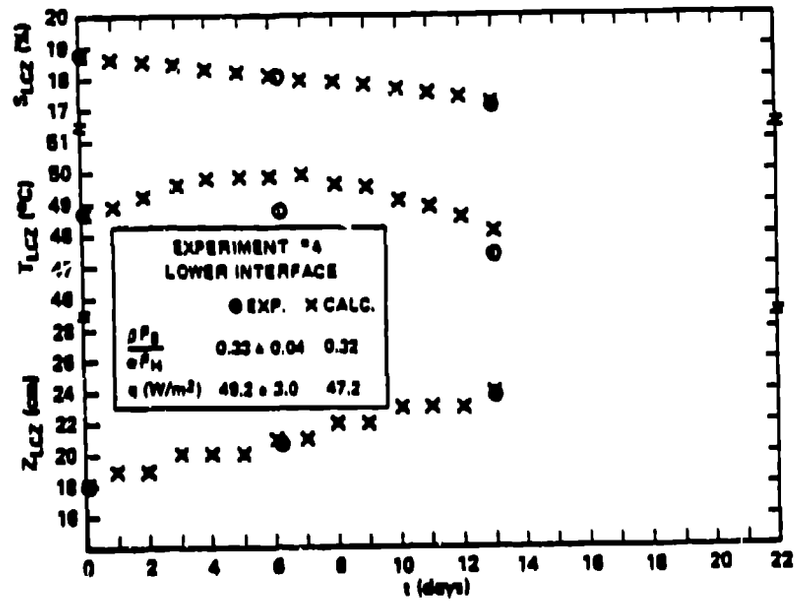

Fig. 18. Comparison of observed and calculated results for laboratory tank experiment number 4. Z = height of boundary layer above pond bottom. $F_H = F_h/\rho c_p$.

TABLE I

RESULTS OF LOS ALAMOS LABORATORY TANK TESTS

Experiment Number	Interface or Zone (Upper/Lower)	Duration (days)	Mixed Zone S_o (%)	Mixed Zone $\Delta S/\Delta t$ (%/day)	Boundary Heat Flux (W/m^2)	Interface Velocity (cm/day)	$\frac{\rho C_p \alpha F_s}{\alpha F_h}$
1*	L	19.00	12.35	0.072	35.2 ± 3.0	0.42	0.26 ± 0.03
2	L	19.04	12.39	0.094	43.2 ± 3.0	0.55	0.35 ± 0.05
2	U	19.04	0.93	-0.084	46.2 ± 3.0	-0.35	0.15 ± 0.04
3	L	22.00	16.30	0.084	61.2 ± 4.0	0.33	0.25 ± 0.03
3	U	22.00	4.27	-0.110	61.2 ± 4.0	-0.15	0.23 ± 0.05
4	L	13.00	18.75	0.126	49.2 ± 3.0	0.45	0.33 ± 0.04
4	U	13.00	1.84	-0.104	49.2 ± 3.0	-0.22	0.16 ± 0.04
5*	L	11.80	11.97	0.115	8.8 ± 0.2	0.017	0.30 ± 0.09

* Performed in dewar. All other results are from insulated flow visualization tank.

The pond had to be cooled in preparation for the experiment; as of May 1, 1983, the LCZ temperature had risen to 55°C. The re-installation of the catwalk and instrumentation (after the leak problems), instrument calibration, and other preparations delayed the start of the experiment.

The pond was cooled by two liquid/air heat exchangers, each with a rated capacity of about 30 kW. Pond temperature profiles for the beginning, middle and end of May, 1983 and the beginning of June are shown in Fig. 19. The suction port for the cooling loop, located near the pond bottom, consisted of a round piece of PVC pipe, 7.6 cm in diameter. The discharge to the LCZ was through a diffuser consisting of two circular acrylic plates, 1 m in diameter with a gap between them 7-mm deep.

For the first half of May, the diffuser position was about 40 cm above the pond floor; the temperature of the pond for May 15 is shown in Fig. 19. After May 15, we moved the diffuser upward to about 70 cm to involve more of the LCZ in the cooling; note in Fig. 19 that the temperature profile on May 31 reflects this change. The rate of heat extraction from the pond varied from 18 to 38 kW during this period. The mean velocity from the diffuser was about 0.2 m/s. The temperature difference between the inlet port and outlet diffuser in the LCZ varied from 5 to 11°C. No measurable boundary erosion occurred although the overall Richardson number (Ri_o defined by Eq. (9)), based on diffuser velocity and distance from diffuser to interface, ranged from 0.2 to 0.95.

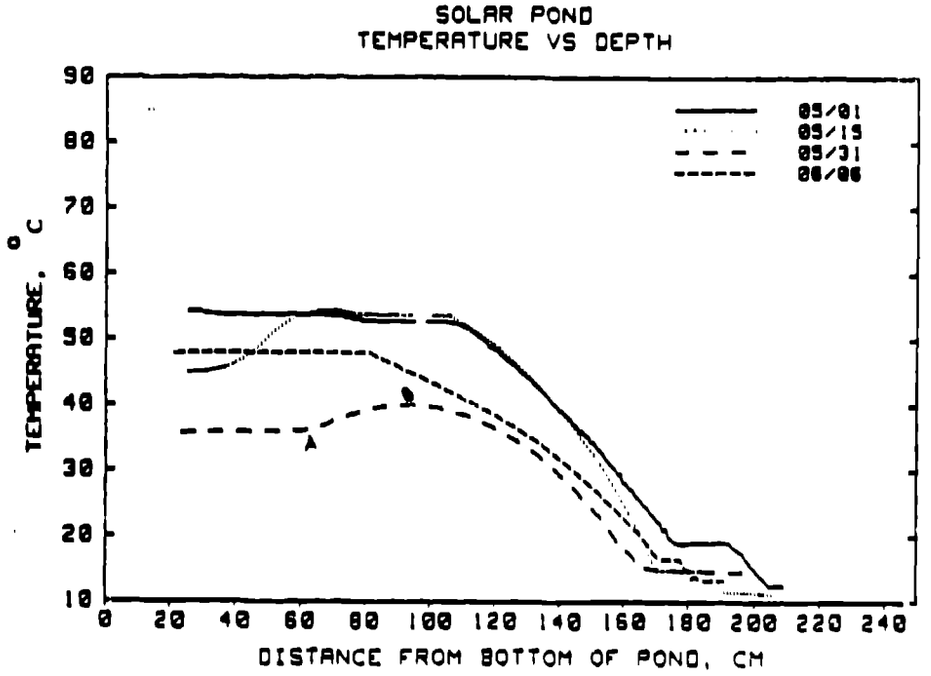

Fig. 19. Temperature Profiles of Solar Pond For Four Days Before Beginning Run-Down Experiment.

From Fig. 19, we also note that between points A and B the pond is stabilized by temperature, this being a region of uniform salinity. From point B to the UCZ boundary, the pond is salinity stabilized. Because diffusion is the only mechanism for salt transport between point A and the UCZ boundary, an increase in the thickness of the diffusive core (gradient zone) results, as shown by a comparison of the temperature profiles for May 1 and June 6.

Unfortunately, the heat exchangers were unable to compete with the combination of daily heat gain in the pond and the stored heat. They were capable of reducing the temperature only to about 36.5°C at the bottom of the pond.

On June 1, as detected in Fig. 19, the top 30 cm of the UCZ was removed and replaced with fresh water to prepare for the run-down experiment. The temperature profiles in the UCZ show this activity. It appears that some erosion of the core occurred during this operation.

Salt water samples were extracted on four days during the run-down for in situ calibration of the conductivity probe. Temperature and salinity profiles in the pond for the days on which the samples were extracted are shown in Figs. 20 and 21, respectively. Salinity was measured by the point-conductivity probe calibrated on the days shown in the figures; temperature was measured with an RTD. On the first

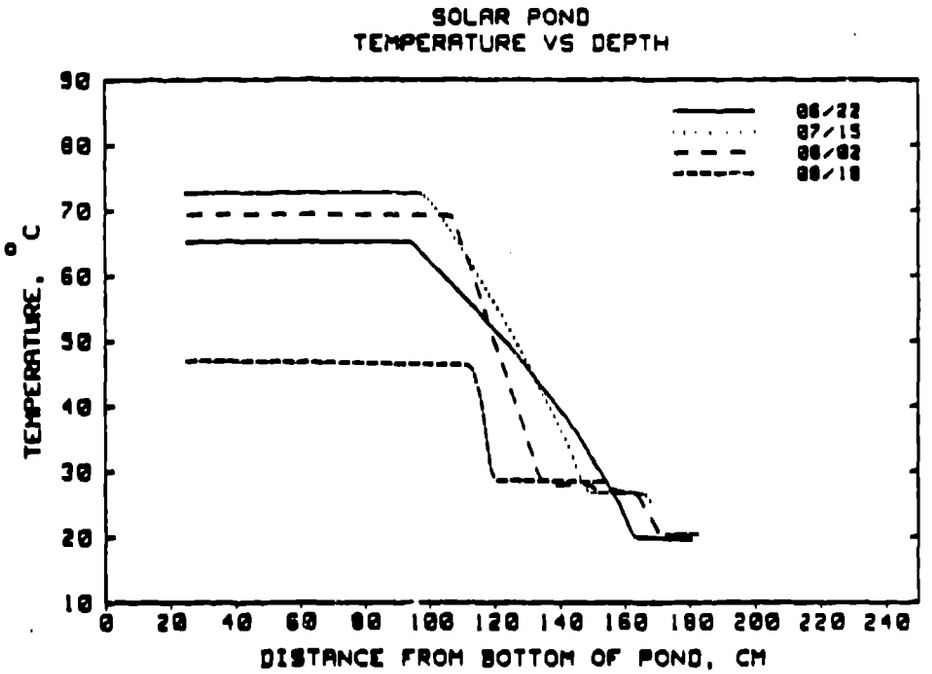

Fig. 20. Temperature Profiles In Pond During Run-down Experiment.

day of extraction, the initial temperature and salinity of the LCZ were 65.1°C and 18.1% respectively. The S-shaped salinity profiles indicate an imbalance between the salt transport rate through the interfaces and the rate of salt diffusion through the core. This behavior persisted until near the end of the experiment, at which time very large rates of salt transport through the core existed.

Fluctuations noted in the salinity profiles in the LCZ (Fig. 21) are not believed to be real, but to be caused by a deteriorating platinum coating on the point-conductivity probe tip. Fortunately, the salinity values for the LCZ used in the salt flux calculations are from extracted samples and not from probe readings.

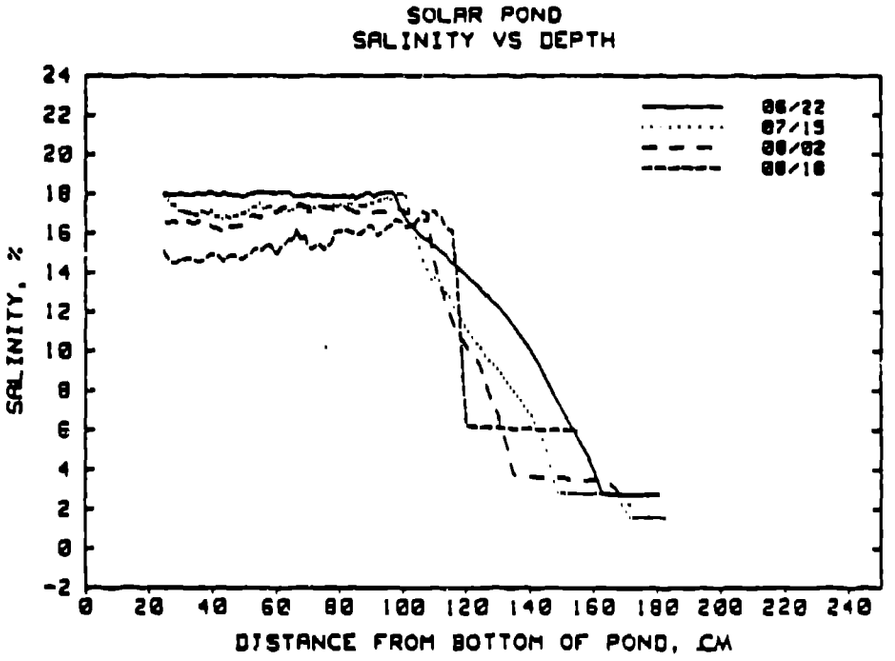

Fig. 21. Salinity Profiles In Pond During Run-Down Experiment.

Flux ratios and other pertinent results from the run-down experiment are presented in Table II. The heat flux at a boundary layer between a mixed zone and the diffusive core was corrected for volumetric heating. This correction was small, however, because the temperature and salinity data were obtained during hours close to sunset.

TABLE II

RESULTS OF LOS ALAMOS SOLAR POND EXPERIMENT

Day of Experiment	Core Thickness (cm)	Average Boundary Salt Flux (g/cm^2-day) LCZ	UCZ	Boundary Heat Flux (W/m^2) LCZ	UCZ	$\frac{\rho C_p \beta F_s}{\alpha F_h}$ LCZ	UCZ	Boundary Velocity (cm/day) LCZ	UCZ	R_ρ
0	70.0									4.94
		0.0207		37.73		0.29		0.13	-0.65	
				±2.74		±0.02				
23	54.0									4.61
		0.0430	0.020	65.71	101.00	0.33	0.220	0.41	-0.73	
				±1.94	±1.88	±0.01	±0.004			
41	29.2									4.66
		0.0719		121.82		0.30		0.25	-0.89	
				±3.91		±0.01				
57	10.8									8.22

From the results presented in Table II, we first note that the rate of run-down was rapid: on the average about 1 cm/day was lost from the core. This is more obvious by inspecting Fig. 22 where the interface locations are shown over the duration of the experiment. We arrived at one possible explanation for the rapid run-down by considering the relatively small values of the overall density-stability ratios shown in Table II. Newell (Ref. 14) indicates that the operational limit of solar ponds corresponds to an R_ρ value of about 7 to 8. Because $R_\rho \approx 5$ for most of the experiment, based on this criterion, the salinity gradient was not large enough to support the temperature gradient and a rapid run-down transpired.

A graph of the temperature in the LCZ during run-down is shown in Fig. 23. In the beginning of June, the rate of warmup was about 1.1°C/day with a core thickness of about 70 cm. We note the rate of temperature decrease to be about three times this value for the end of the experiment when the core thickness was only about 20 cm.

The average salt flux from the LCZ over the first 23 days of the experiment was about 76 kg/m^2-year, and for the second 18 days it was about twice that amount. The smaller number is about 3-1/2 times the maximum measured value for this phenomenon cited by Nielsen and Rabl (Ref. 43). This result is partly

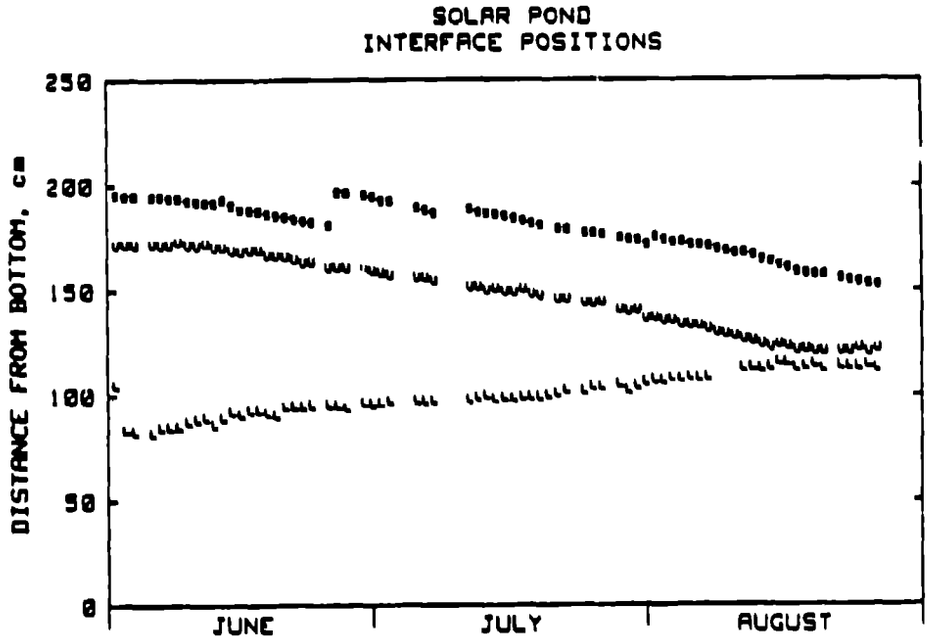

Fig. 22. Locations of the LCZ (l), UCZ (u) interfaces and the surface location (s) in the pond during a run-down experiment.

explained by our measured flux ratios that are larger than Nielsen's (Ref. 42) (see discussion below). Also, the heat fluxes through the interfaces over the course of the run-down experiment were larger than for a pond operated in a quasi-steady mode. The larger heat fluxes then give rise to larger salt fluxes as indicated by Eq. (12).

The consistently larger values of the UCZ interface velocity compared with that at the LCZ, as seen in Table II, may indicate that a leak still exists in the liner at the bottom of the pond. A comparison of evaporation rates measured for the evaporation pond with those in the main pond showed a discrepancy of about 0.4 cm/day over the duration of the experiment. Because of the difference in pond size and bottom reflectivity we suspect this value to be high and the leak rate to be about 0.2 cm/day. Fortunately, because the total leakage over any inventory period is only a small fraction of the volume of the LCZ (< 5%) the effect of a possible leak on the salt flux and flux ratio at the LCZ interface is small. The effect of a possible leak has been accounted for in the error range for the flux ratios shown in Table II.

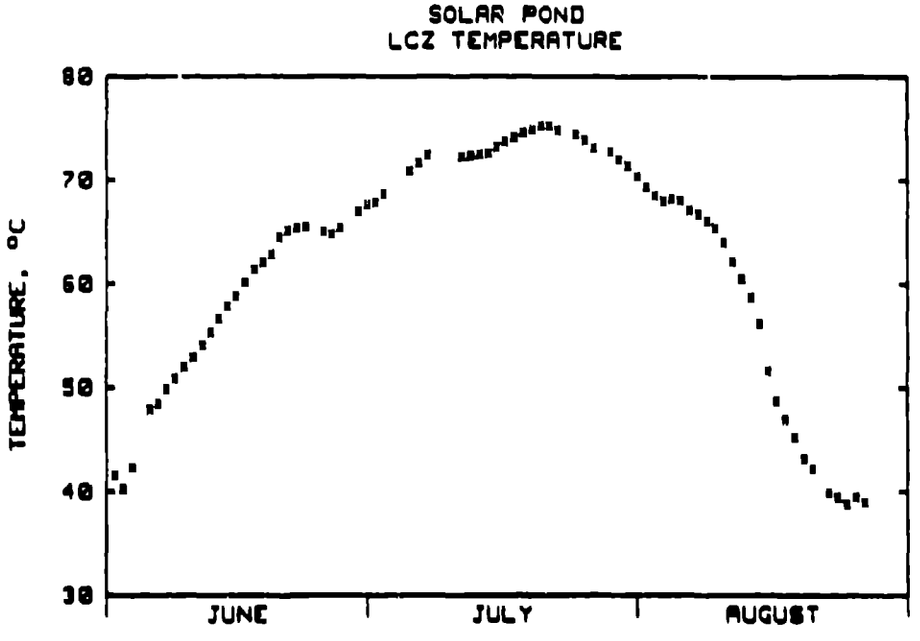

Fig. 23. Temperature of LCZ during the solar pond run-down.

Figure 24 shows the dimensionless salt-to-heat flux ratio with error range as a function of heat flux for our laboratory and pond experiments. We have also included in the figure results from Broughton (Ref. 64) and Marmarino and Caldwell (Ref. 6). We have expressed Nielsen's (Ref. 42) correlation in a form compatable with the Marmarino and Caldwell results and plotted it as a solid curve. In addition, the correlation used by Meyer [Ref. 16 and Eq. (16)] to match the predictions from his numerical model to the Purdue data is shown as a dotted curve. For the Los Alamos data, the partially shaded boxes refer to the results obtained for the LCZ interface and the unshaded boxes refer to the UCZ-interface results. From inspection of Fig. 24, we believe the relatively good agreement supports our conjecture that the same physical phenomena are present in both thermohaline columns and solar ponds. Although the data is scattered, the trend toward a smaller flux ratio at larger heat fluxes is perceptible. In addition, we note that the Nielsen correlation to solar pond data bounds our results from below. We further note the Meyer correlation to be in much better agreement with the data than the Nielsen correlation in the moderate-to-large heat flux range. The relatively good agreement between the flux ratios for the laboratory tank experiments and those from the pond indicates that the effects of convective mixing from bottom heating on salt transport through the LCZ boundary may not be as significant as originally thought. More flux-ratio data for large ponds are needed to answer this question.

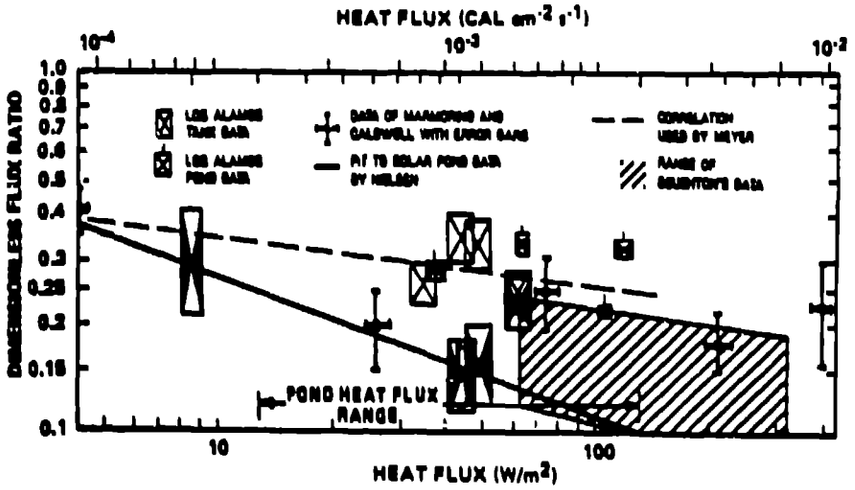

Fig. 24. Dimensionless salt-to-heat flux versus heat flux for pond experiment and laboratory tank tests.

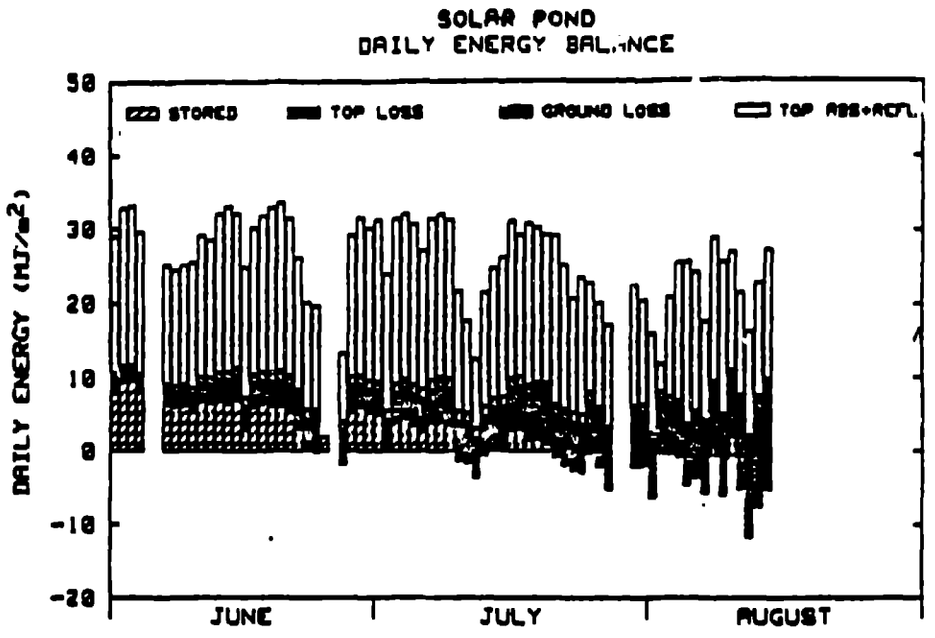

Fig. 25. Energy flows in solar pond. Period of experiment, June 22 through August 18.

It is interesting to compare the results from the run-down experiment with the criteria for stable interfaces proposed by Nielsen and Rabl (Ref. 40) and Newell and Boehm (Ref. 43). From our data we obtain a time-averaged ratio of the difference in salinity to the difference in temperature between the mixed zones of 0.343%/°C. Based on this result, Eq. (5) predicts that the interfaces in the pond are stable whereas a rapid run-down actually occurred. The expression 0.22 $\beta G_s/\alpha G_t$, averaged in time, is about 90 based on our data. Eq. (8) predicts a shrinking of the mixed layers for this value although the actual behavior was quite different.

From these results, it appears the regime of conditions existing in our pond during run-down was quite different from the ones on which the stability criteria were based. More theoretical and experimental work must be done before we are able to develop accurate stability criteria for interfaces in solar ponds.

A bar graph of daily energy flows in the solar pond is shown in Fig. 25 through the end of the run-down experiment. From these results, the average pond efficiency over this period is slightly greater than 20%. Virtually no energy storage occurred in the pond after the middle of July because of the rapid thinning of the core after that time. A tabulation of the daily energy flows is presented in Table III. Symbols are defined in Table IV.

TABLE III

DAILY ENERGY FLOWS DURING THE SOLAR POND RUN-DOWN
****TA46 SOLAR POND DAILY SUMMARY******

JDAY	DATE	QH MJ/m^2	QABS MJ/m^2	QSUCZ MJ/m^2	QSLCZ MJ/m^2	QSSAND MJ/m^2	QSTOT MJ/m^2	QTOP MJ/m^2	QSIDE MJ/m^2	QBOT MJ/m^2	QUNB MJ/m^2	EFF %	TA C	T-UCZ C	T-MCZ C	T-LCZ C
152	830601	28.97	9.08	.36	7.04	.38	7.79	2.92	.06	-.09	-1.61	26.88	13.91	15.45	32.21	39.56
153	830602	32.77	10.04	1.67	7.19	.47	9.33	2.25	.07	.09	-1.69	28.46	15.88	15.74	32.91	41.61
154	830603	33.11	10.13	1.96	6.97	.48	9.40	2.09	.07	.27	-1.71	28.41	15.70	16.44	33.73	43.60
155	830604	29.51	9.19	1.50	6.05	.41	7.96	2.13	.08	.41	-1.38	26.97	17.18	16.52	34.36	45.33
156	830605	0.00	0.00	0.00	0.00	0.00	0.00	0.00	0.00	0.00	0.00	0.00	0.00	0.00	0.00	0.00
157	830606	0.00	0.00	0.00	0.00	0.00	0.00	0.00	0.00	0.00	0.00	0.00	0.00	0.00	0.00	0.00
158	830607	25.15	7.72	1.56	4.30	.32	6.18	2.23	.09	.66	-1.44	24.56	15.29	17.79	35.62	48.71
159	830608	24.46	7.73	1.55	4.02	.30	5.87	2.23	.10	.73	-1.20	24.02	16.90	18.35	36.27	49.86
160	830609	25.13	8.04	1.73	3.97	.30	6.00	2.25	.10	.78	-1.10	23.88	16.55	17.67	37.00	50.99
161	830610	25.52	7.84	1.46	3.51	.29	5.26	2.46	.11	.85	-.83	20.63	16.90	17.84	37.61	51.99
162	830611	29.15	9.06	1.91	4.43	.32	6.66	2.53	.11	.90	-1.14	22.86	20.28	17.85	38.41	53.26
163	830612	28.56	9.03	1.88	4.17	.31	6.37	2.65	.11	.95	-1.05	22.31	17.61	16.60	39.20	54.45
164	830613	32.0[illegible]	9.85	1.59	4.72	.34	6.65	2.97	.12	1.00	-.88	20.74	13.32	14.84	39.87	55.80
165	830614	33.06	10.13	1.27	4.74	.34	6.35	3.34	.12	1.05	-.74	19.21	13.89	15.58	40.40	57.15
166	830615	32.04	9.81	2.07	4.45	.33	6.85	3.33	.13	1.10	-1.61	21.39	18.03	17.07	41.27	58.42
167	830616	24.83	7.61	.64	1.97	.20	2.80	3.30	.13	1.14	.23	11.28	18.63	16.67	41.53	58.98
168	830617	30.24	9.36	1.78	3.84	.28	5.91	3.29	.14	1.16	-1.13	19.54	21.56	17.32	42.28	60.08
169	830618	31.78	9.85	2.07	3.91	.30	6.28	3.27	.14	1.19	-1.03	19.76	22.92	18.61	43.15	61.20
170	830619	32.99	10.12	1.72	3.91	.30	5.93	3.44	.15	1.23	-.63	17.98	23.82	17.80	43.87	62.32
171	830620	33.60	10.30	1.68	3.91	.30	5.89	3.63	.15	1.27	-.64	17.52	23.51	17.39	44.58	63.43
172	830621	31.45	9.72	1.36	3.38	.27	5.01	3.88	.15	1.30	-.63	15.94	23.20	18.41	45.15	64.40
173	830622	26.14	8.25	.60	2.08	.20	2.88	3.97	.16	1.33	-.09	11.04	22.60	19.07	45.40	64.99
174	830623	20.13	6.26	-.56	.56	.10	.10	4.17	.16	1.33	.50	.50	20.20	16.81	45.17	65.15
175	830624	19.68	6.29	-.76	.42	.08	-.25	4.51	.16	1.31	.56	-1.28	15.95	17.11	44.85	65.27
176	830625	0.00	0.00	0.00	0.00	0.00	0.00	0.00	0.00	0.00	0.00	0.00	0.00	0.00	0.00	0.00
177	830626	0.00	0.00	0.00	0.00	0.00	0.00	0.00	0.00	0.00	0.00	0.00	0.00	0.00	0.00	0.00
178	830627	13.31	4.12	-.63	-1.18	-.03	-1.84	4.56	.16	1.20	-.05	-13.13	13.75	18.46	43.23	64.52
179	830628	29.22	9.13	2.75	2.52	.15	5.42	3.51	.16	1.17	-1.13	18.55	17.94	21.09	44.39	65.24
180	830629	31.54	9.76	2.97	2.72	.19	5.87	3.19	.16	1.18	-.64	18.63	20.39	22.39	45.63	66.02
181	830630	30.11	9.41	2.37	2.47	.19	5.03	3.27	.16	1.21	-.27	16.70	22.52	22.86	46.63	66.72
182	830701	31.20	9.67	1.86	2.63	.19	4.68	3.42	.17	1.24	.17	14.99	21.92	22.68	47.40	67.47
183	830702	23.85	7.46	-.34	.73	.09	.48	3.72	.17	1.25	1.83	2.03	21.92	20.99	47.26	67.68
184	830703	31.44	9.71	.53	3.00	.21	3.74	4.07	.17	1.26	.48	11.89	22.36	21.92	47.48	68.54

TABLE III (contd.)

JDAY	DATE	QH MJ/m^2	QABS MJ/m^2	QSMCZ MJ/m^2	QSLCZ MJ/m^2	QSSAND MJ/m^2	QSTOT MJ/m^2	QTOP MJ/m^2	QSIDE MJ/m^2	QBOT MJ/m^2	QUNB MJ/m^2	EFF %	TA C	T-UCZ C	T-MCZ C	T-LCZ C
185	830704	32.09	9.82	.99	3.05	.22	4.26	4.20	.17	1.29	-.11	13.29	23.13	21.96	47.90	69.41
186	830705	30.74	9.45	.49	2.60	.21	3.30	4.34	.18	1.32	.32	10.72	21.87	22.25	48.11	70.15
187	830706	27.06	8.53	.52	1.82	.16	2.50	4.47	.18	1.35	.03	9.25	22.50	22.78	48.32	70.67
188	830707	31.45	9.68	.74	2.71	.20	3.65	4.55	.18	1.36	-.06	11.59	22.92	22.44	48.63	71.45
189	830708	32.00	9.82	.75	2.80	.21	3.76	4.79	.18	1.39	-.30	11.75	23.50	22.75	48.95	72.24
190	830709	31.31	9.69	.55	2.52	.20	3.27	4.98	.19	1.41	-.16	10.45	24.04	23.41	49.18	72.96
191	830710	21.64	6.70	-1.11	-.32	.05	-1.38	5.19	.19	1.43	1.27	-6.36	21.64	22.27	48.71	72.87
192	830711	17.72	5.56	-.84	-.93	-.01	-1.78	5.41	.19	1.41	.34	-10.04	17.05	22.34	48.36	72.61
193	830712	12.49	4.07	-.99	-2.52	-.11	-3.62	5.17	.19	1.35	.98	-29.02	15.56	22.72	47.94	71.89
194	830713	21.51	6.83	-.83	.15	.03	-.66	5.23	.18	1.31	.75	-3.07	17.26	22.23	47.59	71.93
195	830714	24.73	7.80	-.71	.67	.05	.01	5.67	.18	1.30	.64	.04	18.45	21.91	47.29	72.12
196	830715	26.27	8.10	-.63	.75	.06	.19	5.80	.18	1.29	.64	.71	21.68	21.74	47.03	72.34
197	830716	31.11	9.60	.35	2.10	.14	2.59	5.88	.18	1.29	-.34	8.31	23.77	22.61	47.17	72.94
198	830717	29.23	9.13	1.08	1.51	.12	2.70	5.93	.19	1.31	-.99	9.25	22.48	22.61	47.62	73.37
199	830718	30.83	9.53	-.36	1.65	.13	1.42	6.10	.19	1.33	.49	4.60	22.94	23.12	47.47	73.84
200	830719	30.27	9.28	-.24	1.57	.12	1.45	6.49	.19	1.34	-.19	4.80	23.17	22.78	47.37	74.29
201	830720	29.33	9.03	-.27	1.02	.10	.85	6.88	.19	1.35	-.24	2.89	21.56	22.75	47.26	74.58
202	830721	29.14	9.04	-1.98	.97	.09	-.92	5.72	.19	1.36	2.68	-3.15	21.98	22.73	46.42	74.86
203	830722	25.18	7.81	-1.89	-.16	.03	-2.03	6.20	.19	1.36	2.09	-8.04	21.95	22.03	45.63	74.81
204	830723	20.66	6.43	-1.12	-1.60	-.06	-2.78	6.53	.19	1.34	1.14	-13.44	21.73	21.87	45.16	74.36
205	830724	23.47	7.35	-1.70	-1.29	-.05	-3.04	6.54	.19	1.31	2.36	-12.95	21.00	24.63	44.45	73.99
206	830725	22.75	7.31	.25	-.65	-.04	-.43	7.03	.19	1.27	-.74	-1.89	22.33	19.33	44.56	73.80
207	830726	20.03	6.33	-.30	-1.85	-.09	-2.24	6.78	.19	1.25	.36	-11.17	18.13	21.43	44.43	73.28
208	830727	17.07	5.38	-2.38	-2.71	-.15	-5.24	7.11	.18	1.20	2.12	-30.69	18.40	20.77	43.44	72.50
209	830728	0.00	0.00	0.00	0.00	0.00	0.00	0.00	0.00	0.00	0.00	0.00	0.00	0.00	0.00	0.00
210	830729	0.00	0.00	0.00	0.00	0.00	0.00	0.00	0.00	0.00	0.00	0.00	0.00	0.00	0.00	0.00
211	830730	22.32	7.00	-.41	-1.70	-.11	-2.22	7.14	.17	1.11	.80	-9.93	20.90	20.43	42.13	71.49
212	830731	20.36	6.48	.36	-2.39	-.14	-2.17	7.38	.17	1.07	.02	-10.65	20.41	20.36	42.28	70.81
213	830801	15.92	5.00	-2.44	-3.67	-.22	-6.34	7.64	.17	1.02	2.51	-39.81	20.60	17.85	41.25	69.76
214	830802	11.86	3.87	4.33	-4.49	-.28	-.44	7.48	.16	.95	-4.28	-3.70	17.00	19.94	43.07	68.48
215	830803	20.85	6.46	1.44	-1.75	-.15	-.46	6.93	.16	.88	-1.04	-2.19	19.95	21.30	43.67	67.98
216	830804	25.45	7.85	-.55	-.30	-.06	-.91	6.83	.16	.84	.94	-3.59	22.04	22.88	43.44	67.89
217	830805	25.59	7.87	-3.90	-.61	-.06	-4.57	7.33	.15	.83	4.13	-17.86	22.40	22.39	41.81	67.72
218	830806	24.17	7.58	-2.30	-1.33	-.09	-3.72	8.30	.15	.83	2.03	-15.40	21.85	21.68	40.84	67.33
219	830807	17.66	5.70	-1.96	-3.41	-.21	-5.58	8.95	.15	.80	1.39	-31.61	20.12	19.67	40.02	66.36
220	830808	28.82	8.77	.73	-1.37	-.12	-.76	9.40	.15	.76	-.77	-2.65	21.61	22.14	40.33	65.97

TABLE III (contd.)

JDAY	DATE	QH MJ/m^2	QABS MJ/m^2	QSMCZ MJ/m^2	QSLCZ MJ/m^2	QSSAMD MJ/m^2	QSTOT MJ/m^2	QTOP MJ/m^2	QSIDE MJ/m^2	QBOT MJ/m^2	QUNB MJ/m^2	EFF %	TA C	T-UCZ C	T-MCZ C	T-LCZ C
221	830809	25.65	7.95	-3.42	-2.36	-.16	-5.94	10.18	.14	.73	2.84	-23.14	21.82	20.23	38.89	65.29
222	830810	26.99	8.42	1.66	-2.53	-.18	-1.04	11.30	.14	.69	-2.67	-3.86	21.43	21.84	39.59	64.57
223	830811	21.49	6.69	.19	-5.07	-.32	-5.20	12.08	.14	.64	-.98	-24.18	20.69	18.49	39.67	63.12
224	830812	16.23	4.96	-4.67	-6.63	-.43	-11.72	13.17	.13	.56	2.83	-72.25	19.45	20.37	37.71	61.23
225	830813	22.78	7.04	-.81	-6.40	-.44	-7.64	14.68	.12	.44	-.57	-33.54	21.19	21.54	37.38	59.40
226	830814	27.20	8.35	2.03	-6.88	-.47	-5.33	14.63	.11	.33	-1.40	-19.58	22.78	19.34	38.23	57.44
		1792.43	556.93	19.21	65.41	5.80	90.42	382.96	10.60	72.89	-.03	5.05				

TABLE IV

DESCRIPTION OF TERMS IN TABLE III

JDAY - Julian Day

DATE - Year, Month, Day

QH - Integrated daily solar radiation measured with Pyranometer.

QABS - Net solar radiation absorbed after shading and bottom reflection factors. Shading factors were calculated with hourly solar angles. Bottom reflection factor necessary to obtain an energy balance was 0.91.

QSNCZ - Energy stored in non-convecting zone. Calculated with (density x specific heat = 3.975 MJ/m^3) x zone depth x zone temperature daily change.

QSLCZ - Energy stored in lower-convecting zone. (Density x specific heat = 3.891 MJ/m^3) and above equation. Zone depth = 110 cm.

QSSAND- Energy stored in bottom sand layer. (density x specific heat = 1.21 MJ/m^3). Sand depth = 25.4 cm.

QSTOT - Total energy storage. Sum of above 3 terms.

QTOP - Heat loss back to ambient through top surface of pond. Calculated with actual UCZ thickness with daily average temperature difference and K = 0.6 W/m K.

QSIDE - Heat loss through sides of pond. Calculated with average temperature difference of 4 sets of side measurements at 0 and 46 cm depth into earth. K assumed to be 0.5 W/m K.

QBOT - Heat loss at bottom of pond. Calculated with average temperature difference of 2 sets of measurements at 0 and 46 cm depths. K assumed to be 0.85 W/m K.

QUNB - Daily energy unbalance. QABS-QSTOT-QTOP-QSIDE-QBOT.

EFF - Ratio of stored energy (QSTOT) and total horizontal solar energy (QH).

TA - Average daily ambient temperature.

T-UCZ - Average daily upper convecting zone temperature.

T-NCZ - Average daily non-convecting zone temperature.

T-LCZ - Average daily lower-convecting zone temperature.

VI. CONCLUSIONS AND RECOMMENDATIONS FOR FUTURE RESEARCH

A one-dimensional model has been developed that is capable of accurately predicting time-dependent, mixed-zone temperature, salinity, and interface motion.

The correlating parameter in the model is the dimensionless salt-flux-to-heat-flux ratio (flux ratio) as a function of interfacial heat flux. In our experiments, we have obtained 12 values of the flux ratio for heat fluxes ranging from 8 to 100 W/m^2. However, only 4 of the 12 points were obtained from a large pond. More dynamic performance data for large ponds are needed to (1) compare with new theoretical results, (2) complete model validation, and (3) answer the important question of salt replenishment. More data on heat extraction and rejection in actual solar ponds are required to validate the results obtained in laboratory experiments.

The issue of ground loss and its effect on pond performance requires additional attention. A study should be done to determine the effect of ground loss on the overall impact of ponds by considering that future pond sites are restricted to those areas where subsurface conditions permit them to operate efficiently.

Problems continue to exist with pond liners (Ref. 65), methods to determine leak location and in situ repair without disturbing the pond. Divers are not the answer. Research on the physical processes occurring at the boundaries of a linerless pond should be initiated.

The area of instrumentation requires attention. In particular, there is a need for reliable instrumentation to accurately measure fluid specific gravity in situ with a spatial resolution of 0.1 mm and smaller. Accuracy should be 10^{-4} or better. We feel that such an instrument could be developed (Ref. 55). Its measurements would provide data to answer many questions on the fluid dynamics in the immediate neighborhood of a mixed zone/core interface, such as the intermittant entrainment of a dynamic boundary layer.

Some commercially available instruments should be improved. The Beckman induction salinometer installed at the pond failed just before beginning our run-down experiment. Salt water intrusion in the cell was blamed but not proved. Performance of the Eppley 8-48 underwater pyranometer at the pond is suspect because of condensation (or salt water) on the inside of the globe and salt-water attack on the outside of the globe that caused scratches.

VII. DISPOSITION OF EXPERIMENTAL EQUIPMENT

Both tanks and associated hardware are still intact and may be used again without much preparation. The data-acquisition system for the dewar experiment is on permanent loan to another group in the laboratory. It will be difficult to retrieve it.

The pond needs work. If there is a leak in the liner, we suggest that a new liner be installed on top of the old one, which could first be patched and used as a back-up. More salt is needed. Both the underwater pyranometer and the Beckman salinometer need repair. Other instrumentation at the pond remains intact. The data-acquisition system was removed from the pond site but is still available if needed. The traversing mechanism should be modified to eliminate a sticking problem.

ACKNOWLEDGMENTS

This report is the work of many people: D. A. Neeper provided insight and suggestions; K. Hedstrom, C. Bates, and J. Dreicer worked with the experiments; L. Dalton, J. Tafoya, B. Ketchum, L. Brewer, and J. Hauser contributed to the construction of the pond and the experiments.

This study was funded in part by the U.S. Department of Energy, Division of Solar Thermal Energy System and Active Heating and Cooling Division; Office of Solar Heat Technologies; and Office of Solar Applications for Buildings. It was also funded in part by an internal supporting research grant from the Los Alamos National Laboratory.

Nomenclature

c_p	specific heat $(J/g\text{-}^\circ C)$
d	depth of upper convecting zone (cm)
F_s	salt flux $(g/cm^2\text{-}s)$
F_h	heat flux (W/cm^2)
g	acceleration of gravity (cm/s^2)
k_t	thermal conductivity $(W/cm\text{-}^\circ C)$
L	energy extracted at depth of x (W/cm^3)
q	solar energy absorbed at depth x
R_ρ	density-stability ratio
S	salinity (wt. %)
S_0	initial salinity (wt. %)
T	temperature $(^\circ C)$
t^*	time at which thermal boundary layer becomes unstable (s)
t	time (s)
U_e	entrainment velocity (cm/s)
x	vertical coordinate measured from pond bottom (cm)
α	coefficient of thermal expansion $(^\circ C^{-1})$
β	salinity expansion coefficient (cm^3/g)
κ_t	thermal diffusivity (cm^2/s)
κ_s	salt diffusivity (cm^2/s)
ν	kinematic viscosity (cm^2/s)
ρ	fluid density (g/cm^3)
ρ_s	solute density (g/cm^3)

REFERENCES

1. R. Viskanta and J. S. Toor, "Absorption of Solar Radiation in Ponds," Journal of Solar Energy, 21, 59 (1978).

2. A. Rabl and C. E. Nielsen, "Solar Ponds for Space Heating," Journal of Solar Energy, 17, 1 (1975).

3. M. N. A. Hawlader, "The Influence of the Extinction Coefficient," Journal of Solar Energy, 25, 461 (1980).

4. H. E. Huppert and J. S. Turner, "Double Diffusive Convection," Journal of Fluid Mechanics, 106, 299 (1981).

5. P. F. Crapper, "Measurements Across a Diffusive Interface," Deep Sea Research, 22, 537 (1975).

6. G. O. Marmarino and D. R. Caldwell, "Heat and Salt Transport Through A Diffusive Interface," Deep Sea Research, 23, 59 (1976).

7. W. R. Lindberg and R. D. Haberstroh, "A Thermohaline Convection Model," Office of Naval Research Project NR-083-250, Tech. Report No. 1 (November 1971).

8. P. F. Linden and T. G. L. Shirtcliffe, "The Diffusive Interface in Double Diffusive Convection," Journal of Fluid Mechanics, 87, 417 (1978).

9. E. M. Sparrow, R. B. Husar, and R. J. Goldstein, "Observation and Other Characteristics of Thermals," Journal of Fluid Mechanics, 41, 793 (1970).

10. L. N. Howard, "Convection at High Raleigh Number," Proc. 11th International Congress of Applied Mechanics, Munich, 1964 (Springer-Verlag, Berlin, 1964).

11. J. S. Turner," The Coupled Turbulent Transports of Salt and Heat Across A Sharp Density Interface," Int. Jour. of Heat and Mass Transfer, 8, 759 (1965).

12. J. S. Turner," The Behavior of a Stable Salinity Gradient Heated From Below," Journal of Fluid Mechanics, 33, 183 (1968).

13. T. A. Newell and P. M. Von Driska, "Double Diffusive Convection Across a Single Interface at High Density Stability Ratio." Natural Convection in Enclosures - 1983, ASME HTD-Vol. 26, 1983 (American Society of Mechanical Engineers, New York, 1983).

14. T. A. Newell, "Characteristics of a Double Diffusive Interface at High Density Stability Ratios," submitted to Journal of Fluid Mechanics.

15. T. R. Mancini, R. I. Loehrke, and R. D. Haberstroh, "Layered Thermchaline Natural Convection," Journal of Heat and Mass Transfer, 19, 839 (1976).

16. K. A. Meyer, "A Numerical Model to Describe the Layer Behavior in Salt-Gradient Solar Ponds," Journal of Solar Energy Engineering, 105, 341 (1983).

17. H. Weinberger, "The Physics of The Solar Pond," Journal of Solar Energy, 8, 45 (1964).

18. G. Veronis, "On Finite Amplitude Instability in Thermohaline Convection," Journal of Marine Research, 23, 1 (1965).

19. G. Veronis, "Effect of a Stabilizing Gradient of Solute on Thermal Convection," Journal of Fluid Mechanics, 34, 315 (1968).

20. P. G. Baines and A. E. Gill, "On Thermohaline Convection with Linear Gradients," Journal of Fluid Mechanics, 37, 287 (1969).

21. J. S. Turner, "Double Diffusive Phenomena, "Ann. Rev. of Fluid Mechanics, 6, 37 (1974).

22. J. S. Turner, Lecture Presented at the Double-Diffusive Convection Conference, Santa Barbara, California, March 14-18, 1983.

23. R. Almanza and H. C. Bryant," Oscillatory Motions in the Non-Convective Layer of a Solar Pond," Journal of Solar Energy Engineering, 105, 375 (1983).

24. D. P. Grimmer and G. F. Jones, "Preliminary Evidence for Internal Wave Motion at Boundaries of Convecting and Non-convecting Zones in Layered Thermohaline Columns," International Comm. Heat Mass Transfer, 11, 283 (1984).

25. C. E. Nielsen, "Design and Initial Operation of a 400m^2 Solar Pond," Proc. International Solar Energy Society Meeting, Phoenix, Arizona, 1980 (International Solar Energy Society, Newark, Delaware, 1980), p. 381.

26. C. E. Nielsen, "Salt Transport and Gradient Maintenance in Solar Ponds, Proc. International Solary Energy Society Meeting, Houston, Texas, 1982 (International Solar Energy Society, Newark, Delaware, 1982), p. 179.

27. F. Zangrando and J. Green, "On Heat and Mass Exchange in a Partially Stratfied Fluid," to be presented at the 22nd National Heat Transfer Conference, Niagara Falls, New York, August 5-8, 1984.

28 T. L. Bergman, F. P. Incropera, and R. Viskanta, "A Multi-Layer Model for Fixing Layer Development in a Double-Diffusive Thermohaline System Heated from Below," International Journal of Heat and Mass Transfer, 25, 1411 (1982).

29. P. F. Crapper, "Fluxes of Heat and Salt Across a Diffusive Interface in the Presence of Grid-Generated Turbulence," International Journal of Heat and Mass Transfer, 19, 1371 (1976).

30. J. S. Turner, "The Influence of Molecular Diffusivity on Turbulent Entrainment Across a Density Interface, "Journal of Fluid Mechanics, 33, 639 (1969).

31. J. F. Atkinson and D. R. F. Harleman, "A Wind-Mixed Layer Model for Solar Ponds," Journal of Solar Energy, 31, 243 (1983).

32. Y. S. Cha, W. T. Sha, and W. W. Schertz, "Modeling Surface Convective Layer of Salt-Gradient Solar Ponds," Journal of Solar Energy Engineering, 104, 293 (1982).

33. C. F. Kooi, "Salt Gradient Solar Pond With Reflective Bottom Application to 'Saturated' Pond," Journal of Solar Energy, 26, 113 (1981).

34. C. F. Kooi, "The Steady State Salt Gradient Solar Pond," Journal of Solar Energy, 23, 37 (1979).

35. J. R. Hull, "Calculation of Solar Pond Theoretical Efficiency With A Diffusively Reflecting Bottom," Journal of Solar Energy, 29, 385 (1982).

36. J. R. Hull, "Computer Simulation of Solar Pond Thermal Behavior," Journal of Solar Energy, 25 33 (1980).

37. S. A. Shah, T. H. Short, and R. P. Flynn, "Modeling and Testing a Salt Gradient Solar Pond in Northeast Ohio," Journal of Solar Energy, 27, 393 (1981).

38. R. P. Flynn and T. H. Short, "Solar Ponds - A Basic Manual," Special Circular 106, The Ohio State University, OARDC, Wooster, Ohio (February 1983).

39. M. Edesses, J. Henderson, and T. S. Jayadev, "A Single Design Tool for Sizing Solar Ponds," Solar Energy Research Institute report, SERI RR-351-347 (December, 1979).

40. T. A. Newell and R. F. Boehm, "Gradient Zone Constraints in a Salt-Stratified Solar Pond," Journal Solar Energy Engineering, 104, 280 (1982).

41. C. E. Nielsen, "Equilibrium Thickness of The Stable Gradient Zone in Solar Ponds," Proc. International Solar Energy Society Meeting, Denver, Colorado, August, 1978 (International Solar Energy Society, Newark, Delaware 1978), p. 932.

42. C. E. Nielsen, "Control of Gradient Zone Boundaries," Proc. International Solar Energy Society Meeting, Atlanta, Georgia, May 28, 1979 (International Solar Energy Society, Newark, Delaware, 1979), p. 1010.

43. C. E. Nielsen and A. Rabl, "Salt Requirement and Stability of Solar Ponds," Proc. Joint Conference International Solar Energy Society and Solar Energy Society of Canada, Inc., Winnepeg, Ontario, August 15-20, 1976 (International Solar Energy Society, Newark, Delaware, 1976).

44. C. E. Nielsen, "Surface Zone Behavior in Solar Ponds," American Society of Mechanical Engineers paper no. 82-WA/SOL-25, (American Society of Mechanical Engineers, New York, 1982).

45. Y. Jaluria, "Heat Rejection and Energy Extraction Within Solar Ponds," Solar Energy Research Institute report, SERI/PR-252-1393 (February 1982).

46. Y. Jaluria and C. K. Cha, "Heat Rejection to the Surface Layer of a Solar Pond," American Society of Mechanical Engineers paper no. 83-HT-77, 1983.

47. K. A. Meyer and J. C. Hedstrom, "Estimates of Ground Conductivity for the DOE-USAFA Experimental Solar Pond," Los Alamos National Laboratory report LA-UR-82-2904 (1982).

48. C. Leboeuf and D. H. Johnson, "Effects of Soil Condition on Solar Pond Performance," Proc. ASME-SED Sixth Annual Technical Conference, Las Vegas, Nevada, April 8-12, 1984 (American Society of Mechanical Engineers, New York, 1984).

49. D. A. de Vries, "Simultaneous Transfer of Heat and Moisture in Porous Media," Trans. Am. Geophysical Union, 39, 909 (1958).

50. [illegible] R. Walker, J. D. Sabey, and D. R. Hampton, "Studies of Heat Transfer and Water Migration in Soils," Report DOE/CS/30139-TI, Colorado State University, Fort Collins, Colorado, (April 1981).

51 M. Rothmeyer, "The Soret Effect and Salt-Gradient Solar Ponds," Journal of Solar Energy, 25, 567 (1980).

52 K. A. Meyer, D. P. Grimmer, and G. F. Jones, "An Experimental and Theoretical Study of Salt-Gradient Solar Pond Interface Behavior," Proc. International Solar Energy Society Meeting, Houston, Texas, 1982 (International Solar Energy Society, Newark, Delaware, 1982), p. 185.

53. D. P. Grimmer, G. F. Jones, J. Tafoya and T. J. Fitzgerald, "Development of a Point-Electrode Conductivity Salinometer with High Spatial Resolution for Use In Very Saline Solutions," Rev. of Sci. Instrum., 54, 1744 (1983).

54. G. F. Jones, D. P. Grimmer, J. Tafoya and T. J. Fitzgerald, "Development of a Point-Electrode Conductivity Salinometer with High Spatial Resolution for Use In Very Saline Solutions," Proc. International Solar Energy Society Meeting, Minneapolis, Minnesota, June 1983, (International Solar Energy Society, Newark, Delaware, 1983).

55. D. P. Grimmer, G. F. Jones, J. Tafoya, and T. J. Fitzgerald, "Development of a Point-Electrode Conductivity Salinometer with High Spatial Resolution for Use In Very Saline Solutions," Los Alamos National Laboratory report LA-9654-MS (1983).

56. V. Gartner, "Visualization of Particle Displacement and Flow in Stratified Salt Water," Exp. Fluids, 1, 55 (1983).

57. D. J. Baker, "A Technique for the Precise Measurement of Small Fluid Velocities," Journal of Fluid Mechanics, 87, 417 (1978).

58. G. F. Jones, K. A. Meyer, J. C. Hedstrom, J. S. Dreicer, and D. P. Grimmer, "Design, Construction, and Initial Operation of the Los Alamos National Laboratory Salt-Gradient Solar Pond," Proc. ASME-SED Meeting, Orlando, Florida, April 19-21, 1983 (American Society of Mechanical Engineers, New York, 1983), p.157.

59. G. F. Jones and K. A. Meyer, "Description and Initial Operation of the Los Alamos National Laboratory Salt-Gradient Solar Pond," Los Alamos National Laboratory report LA-UR-82-2694 (October, 1982).

60. C. J. Poplowsky, "Laboratory Simulation of the Solar Pond: Double Diffusive, Thermohaline Systems," Masters Thesis, Purdue University, Department of Mechanical Engineering, 1980.

61. J. Wu "Wind-Induced Turbulent Entrainment Across A Stable Density Interface," Journal of Fluid Mechanics, 61, 275 (1973).

62. E. Kit, E. Berent, and M. Vajada, "Vertical Mixing Induced by Wind and Rotating Screen In A Stratified Fluid In A Channel," Journal Hydraulic Research, 18, 35 (1980).

63. D. L. Elwell, T. A. Short, and P. C. Badger, "Stability Criteria for Solar (Thermal-Haline) Ponds," Proc. International Solar Energy Society Meeting, Orlando, Florida, June 6-10, 1977 (International Solar Energy Society, Newark, Delaware, 1977) p. 29 (No. 16).

64. J. M. Broughton, "Experiments on Steady Layered Convection in a Doubly Diffusive System," Masters Thesis, Colorado State University, Department of Mechanical Engineering, 1972.

65. Bill Irwin, TVA, personal communication, April, 1984.